# GNSS time series and velocities about a slow convergent margin processed on HPC clusters: products and robustness evaluation

Lavinia Tunini[1], Andrea Magrin[1], Giuliana Rossi[1], David Zuliani[1]

[1]National Institute of Oceanography and Applied Geophysics - OGS, Trieste-Udine, Italy

5    *Correspondence to*: Lavinia Tunini (ltunini@ogs.it)

**Abstract.** Global Navigation Satellite Systems are well-known fundamental tools for crustal monitoring projects and tectonic studies, thanks to the high coverage and the high-quality data. In slow convergent margins, in particular, where the deformation rates are of the order of few mm/yr, ~~the~~ GNSS monitoring ~~is~~ beneficial ~~to detect~~ the diffused deformation ~~which is~~ responsible for the tectonic stress accrual. Its strength ~~is~~ the high precision reached by GNSS permanent stations, particularly if long ~~span~~

10    data and stable monuments are available at all the stations. North-East Italy is a region which can take the most from continuous and high-precision geodetic monitoring, since it is a tectonically active region located in the northernmost sector of the Adria microplate, slowly converging with the Eurasia plate, but characterised by low deformation rates and moderate seismicity. Furthermore, this region is equipped with a permanent GNSS network providing real-time data and daily observations over two decades. The Friuli Venezia Giulia Deformation Network (FReDNet) was established in the area in 2002 to monitor crustal

15    deformation and contribute to the regional seismic hazard assessment. This paper describes GNSS time series spanning two decades of stations located in the NE-Italy and surroundings, as well as the outcoming velocity field. The documented dataset has been retrieved by processing the GNSS observations with the GAMIT/GLOBK software ver10.71, which allows calculating high-precision coordinate time series, position and velocity for each GNSS station, and by taking advantage of the high-performance computing resources of the Italian High-Performance Computing Centre (CINECA) clusters.

20    The GNSS observations (raw and standard RINEX formats) and the time series estimated with the same procedure are currently daily continued, collected and stored in the framework of a long-term monitoring project. Instead, velocity solutions are planned to be updated annually. The time series and velocity field dataset documented here is available at https://doi.org/10.13120/b6aj-2s32 (Tunini et al., 2023).

## 1 Introduction

25    The Global Navigation Satellite Systems (GNSS) provide a globally-extended dataset which is a milestone not only for crustal deformation and tectonic studies but also for plenty of applications going from surveying to metrology and hazard monitoring projects in the environmental sciences. In recent years, the GNSS technology has been continuously and rapidly growing, with multi-constellation and multi-frequency signals supported by cutting-edge processing algorithms devoted to the integration of different sensors (sensor fusion techniques) and improvements in error mitigation procedures. The well-known GPS, combined

30    with GLONASS and the more recent Galileo and Beidou constellations, can provide the position of a GNSS sensor with a

precision that reaches a few millimetres if long-span data, precise satellite orbits, and stable monuments at the stations are available.
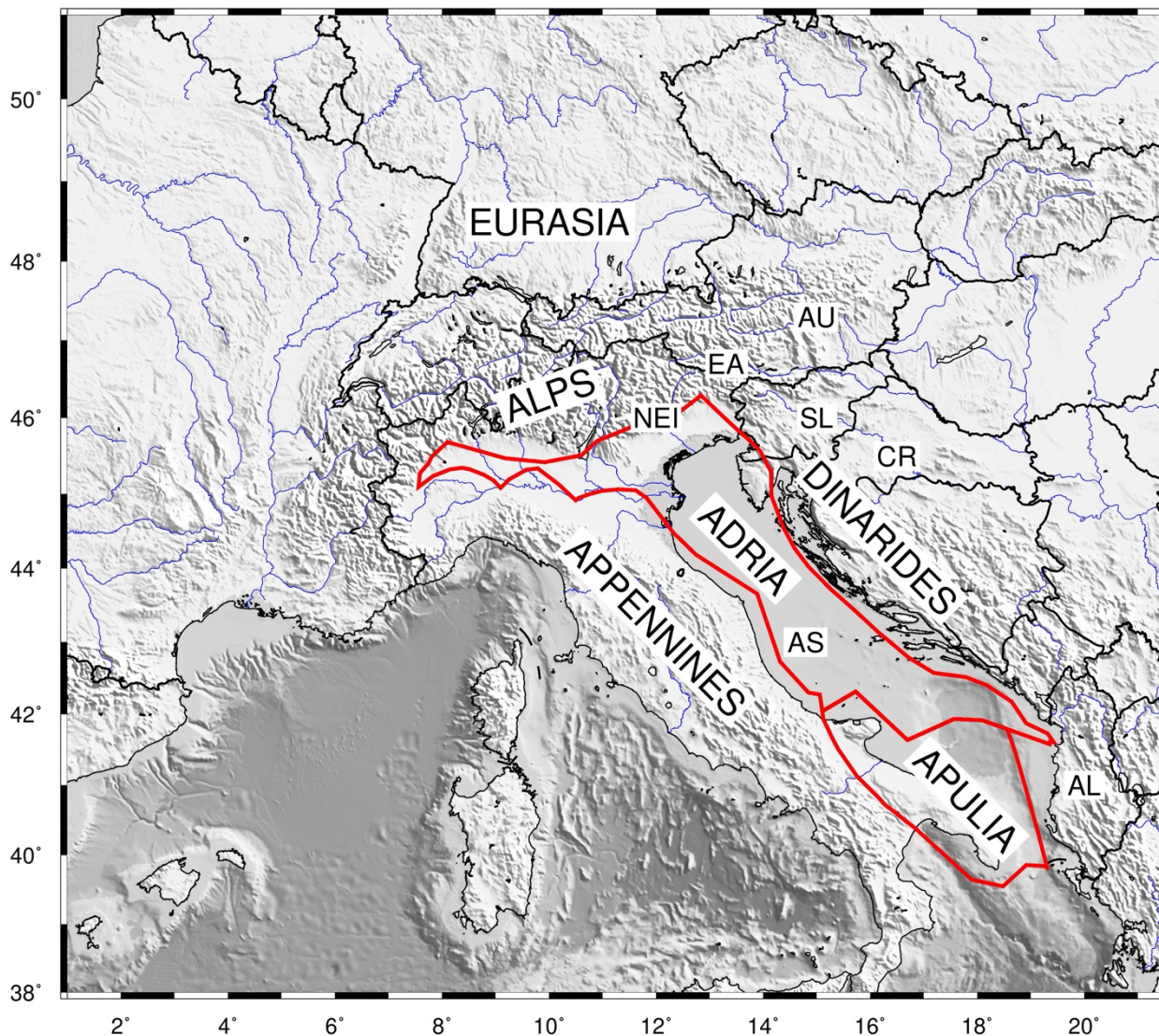
**Fig. 1: Map of the study area, with topography from ETOPO1 (Amante and Eakins, 2009). Red lines indicate the boundary of the Adria microplate; we refer to the "Adria microplate" as the Adriatic sea plate domain, also including the Apulia block in the southern Adriatic sea. Continental lithosphere polygons from GPlates 2.1 dataset (https://www.earthbyte.org/gplates-2-1-software-and-data-sets/) are in agreement with Mathews et al. (2016). AL: Albania; AS: Adriatic Sea; AU: Austria; CR: Croatia; EA: Eastern Alps; NEI: North-East Italy; SL: Slovenia.**

40    Notwithstanding the availability of reliable and consistent GNSS solutions at global scales, such as, e.g. the ones provided by Nevada geodetic Laboratory (http://geodesy.unr.edu/), at regional scales, it can be preferable to consider an ad-hoc reference frame and to tune the processing scheme, in order to obtain high quality time series and high-quality velocity field in regions of particular interest. North-East Italy (Fig. 1) is a particularly suitable region, since a high number of GNSS stations from different agencies have been deployed to monitor the deformations since the beginning of the century. North-East Italy lies at

45    the northern edge of the Adria microplate, a continental lithosphere block, part of the distributed deformation zone between the African and Eurasian plates, encompassing the eastern Italian peninsula from Sicily to the border with Austria and Slovenia, and the eastern Adriatic coast from Slovenia to Croatia and Albania (Battaglia et al., 2003). Adria microplate is recognized to have a counterclockwise motion, implying its collision with Eurasia along its northern tip (Battaglia et al., 2003; D'Agostino et al., 2005, 2008; Serpelloni et al., 2005). The convergence between Adria and Eurasia plates leads to significant consequences

50    on the deformation of the NE-Italy, as revealed by the moderate seismicity, primarily concentrated in the southern sector of the Eastern Alps, and diffused tectonic deformation (Castellarin and Cantelli, 2000; Bressan et al., 2021). Although the deformation rates (2–3 mm/yr of N-S shortening; D'Agostino et al., 2005; Weber et al., 2010; Devoti et al., 2011) remain quite low, if compared to fast converging margins like India-Eurasia or Arabia-Eurasia, this is the most seismic active area of the entire Alps chain. Hence, ~~North-East~~ Italy is ~~essential~~ in understanding the Adria Plate geodynamics (Brancolini et al., 2019;

55    Magrin and Rossi, 2020). The deformation in the area is currently monitored through GNSS instruments by the National Institute of Oceanography and Applied Geophysics - OGS, the Friuli Venezia Giulia regional council and other entities, providing new and denser data to the information available since the 60s of the XX century from the NE-Italy subsurface tilt and strainmeter network (Braitenberg and Zadro, 1999, Rossi et al., 2021). The Friuli Venezia Giulia Deformation Network (FReDNet) is the GNSS network installed by OGS to monitor the crustal deformation distribution ~~of~~ and provide

60    supplementary information for the regional earthquake hazard assessment (Zuliani et al., 2018). It is currently counting 22 permanent GNSS stations providing data on the scale of 15-20 km in most of the region and covering a more than 15 years-long period for the majority of the stations (more details in Appendix A). FReDNet is part of the North-East Italy seismic and geodetic monitoring system (Sistema di Monitoraggio terrestre dell'Italia Nord Orientale - SMINO) of OGS, which also includes seismic broad-band and short and mean period stations, as well as strong motion stations (Bragato et al., 2021 and

65    references therein).

In this paper, we document a dataset of coordinate time series, positions and velocities for 350 stations in NE-Italy and surroundings, whose data have been continuously collected over the past two decades. Data have been processed taking advantage of the high-performance computing resources offered by CINECA (https://www.hpc.cineca.it/) clusters through the Italian SuperComputing Resource Allocation - ISCRA initiative, and through the resources available inside the HPC Training

70    and Research for Earth Sciences (HPC-TRES) program, co-sponsored by the Minister of Education, University and Research (MIUR). The HPC-TRES training program, drown-up by OGS and CINECA, is targeted to promote advanced training in the fields of Earth System sciences and enhance human resources and capacity building through the use of national and European HPC infrastructures and services in the framework of the international infrastructure PRACE - The Partnership for Advanced

Computing in Europe (https://prace-ri.eu/). In Section 2 and in Section 3, we describe the collected input data and the elaboration procedure, respectively. Finally, the dataset of time series and velocities is presented in Section 4, whereas Section 5 illustrates some experiments to evaluate the dataset's quality and robustness. Section 6 provides information on the data availability and Section 7 outlines some final considerations.

The dataset has the potential to provide high-quality and updated information relative to an active but slow converging margin. The elaboration procedure required to produce the dataset has been designed and performed by taking into consideration and eventually correcting each slight bias or parameter selection error which can compromise the quality of the results and/or cause a deviation of the small velocities estimate.

## 2 Input data

We considered the data recorded by all available permanent GNSS stations located in North-East Italy and surrounding regions (Fig. 2). These stations belong to different networks: the OGS geodetic network FReDNet (http://frednet.crs.ogs.it/DOI/); the GNSS network Antonio Marussi of the Friuli Venezia Giulia (FVG) regional council, with stations located throughout the FVG region, hence enhancing the coverage offered by FReDNet sites (Marussi); the Veneto region GPS network (VNTO); the Servizio di Posizionamento SPIN3 GNSS (SPIN), a network covering Lombardia, Piemonte and Valle D'Aosta regions; the South Tyrolean Positioning Service (STPOS) and Trentino POsitioning Service (TPOS), which are the geodetic networks of the Autonomous Provinces of Trento and Bolzano, respectively; the Liguria region GNSS network (LIGU); the Rete Nazionale Integrata GNSS (RING) belonging to the National Institute of Geophysics and Volcanology (INGV); the Nuova Rete Fiduciale Nazionale GNSS of the Italian Space Agency (ASI); the EUREF Permanent Network (EPN), which includes stations managed by different institutions; the Echtzeit Positionierung Austria (EPOSA) network; the SIGNAL network of the Geodetic Institute of Slovenia (SIGN) and other Slovenian GNSS sites acquired by OGS in agreement with the University of Ljubljana and the non-profit organisation Zavod MPRI, raziskovalna in razvojna dejavnost (previously with the Slovenian company Harphasea) (in the following: SLO_GPS). Although some of these networks were designed for cadastral and civil purposes, the validity of such data for velocity estimates has been demonstrated in several works since the benefit of redundancy and increased spatial density overcomes the noise eventually present (Serpelloni et al., 2022 and references therein).
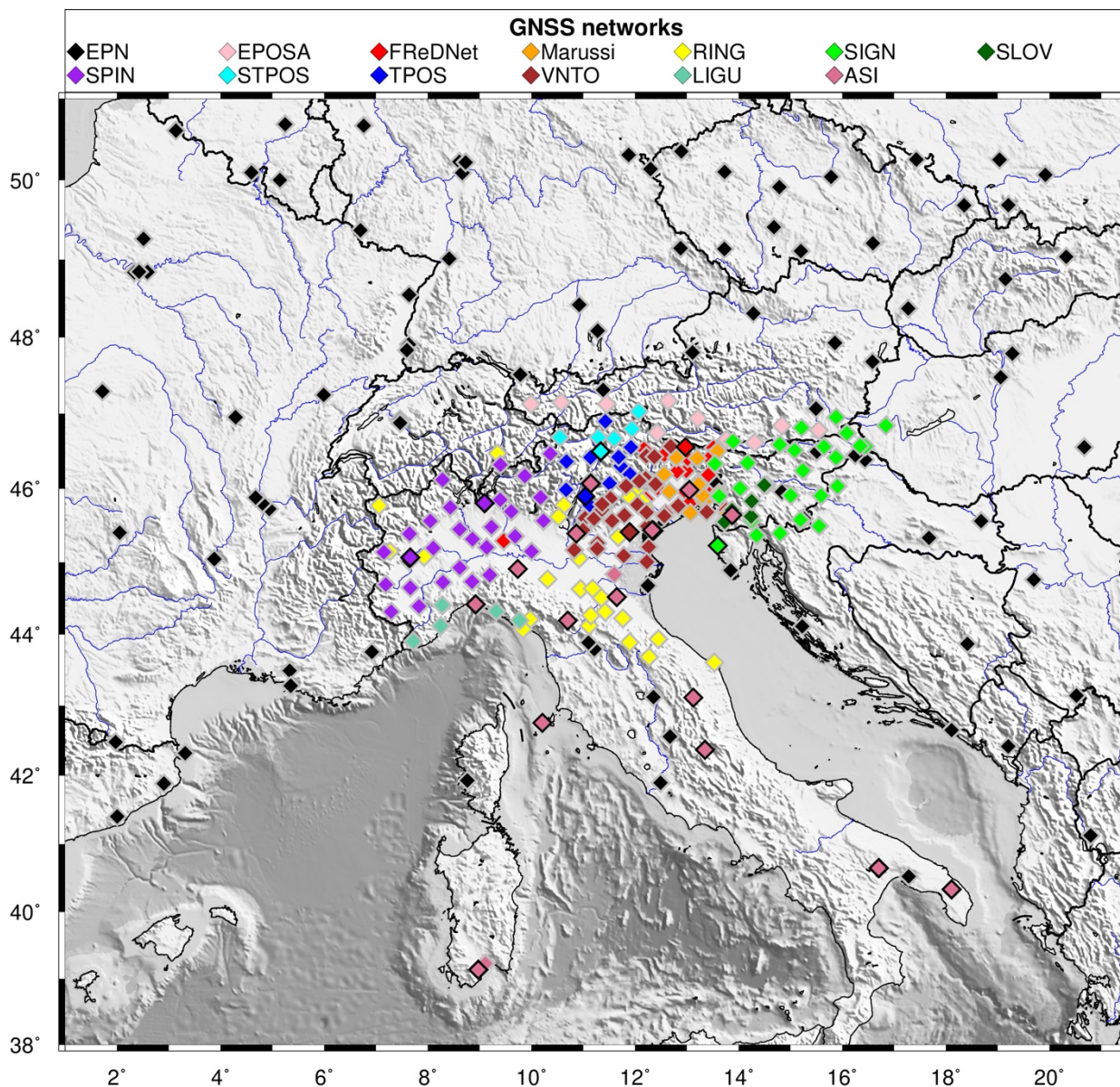
**Fig 2: GNSS stations location and belonging ~~network~~. Symbols contoured by black lines indicate the stations which belong to a regional network but also to European network EPN. In the legenda the explanation of the colours used for the different networks (see the text for the abbreviations).**

In order to link our solutions to the international reference frame ITRF14, we also consider the data coming from reference stations belonging to EPN and IGS networks. In a rectangular area going from 39.75°N to 50.70°N latitude and from 1.5° to 21°E longitude and centred in N-E Italy, whose size has been empirically selected to obtain a stable position-velocity solution

for each of the target stations, we consider as reference stations all the EPN and IGS sites located inside it, adding four more EPN sites located in Sardinia (CAGL, CAG1, CAGZ and UCAG) to improve the coverage in the southern sector. ~~Although we consider~~ more than 350 stations ~~inside the study~~ area ~~overall in this work~~ (5 stations - GUMM, LECC, LEIB, RUDI, SILL

110 - were moved more than 1 m from the original position; therefore, we renamed them), ~~the number of data available is sensibly inferior, progressively increasing from some tens of data/day available in 2002 to approximately 250 data/day available since 2011~~ (Fig. 3). The data availability highly depends on station operability, remote connection functioning, and decommissioning/installation of stations.

The total number of the daily observation files processed in this study is about 0.57 million.

115
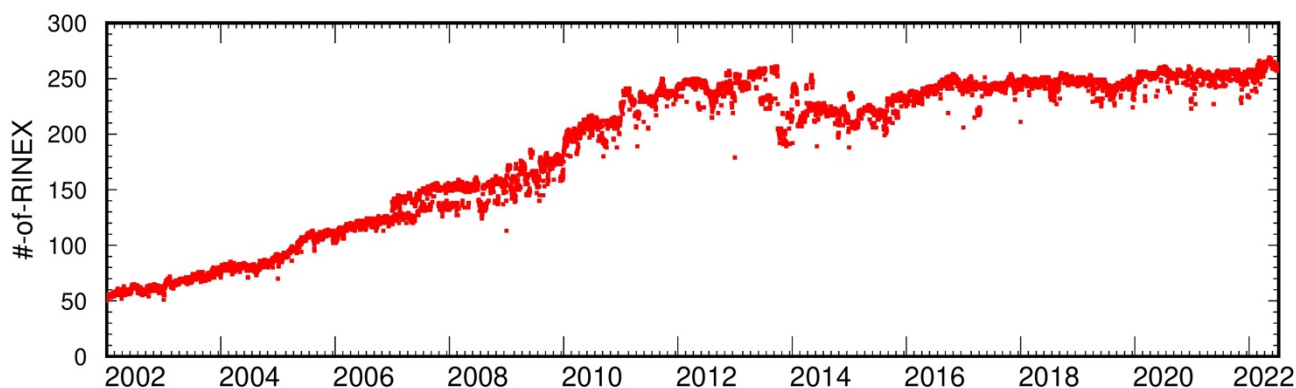
**Fig. 3: Amount of data available with time.**

We have collected GNSS observation data since 2002, 1st January. Raw data from the FReDNet network are collected, quality-

120 checked, transformed into the Receiver INdependent EXchange (RINEX) format, and then released, through a public ftp repository, as hourly and daily files at both 1s and 30s sampling. Data from EPOSA network and SLO_GPS stations are collected in real-time through the GNSMART software (Gerhard et al., 2001) and then converted into RINEX format for post-processing. Finally, RINEX-formatted data deriving from the other networks are collected using different services of data distribution: public data repository of the networks, EPN data distribution services and European Plate Observation System

125 (EPOS) service (Fig. 4).

Like the SMINO monitoring system to which it belongs, FReDNet network aims to provide a monitoring service on a long-term basis. Hence, raw observations and RINEX-formatted data from FReDNet stations are currently continuously retrieved, collected and stored in the OGS internal repository on hourly and daily basis (FReDNet Data Centre, FReDNet DC 2016), where also real-time observations are available. FReDNet data are distributed under a Creative Common licence (CC BY-SA)

130 and accessible at the link https://frednet.crs.ogs.it/DOI/. They are allocated into folders according to the sampling interval (RINEX 30s or RINEX 1s, for 30 seconds or 1 second sampled observations, respectively), year and ~~day of the year~~ (doy) of

the acquisition. From the same web page https://frednet.crs.ogs.it/DOI/, metadata of FReDNet sites are also retrievable by clicking on the "log sheets" link.
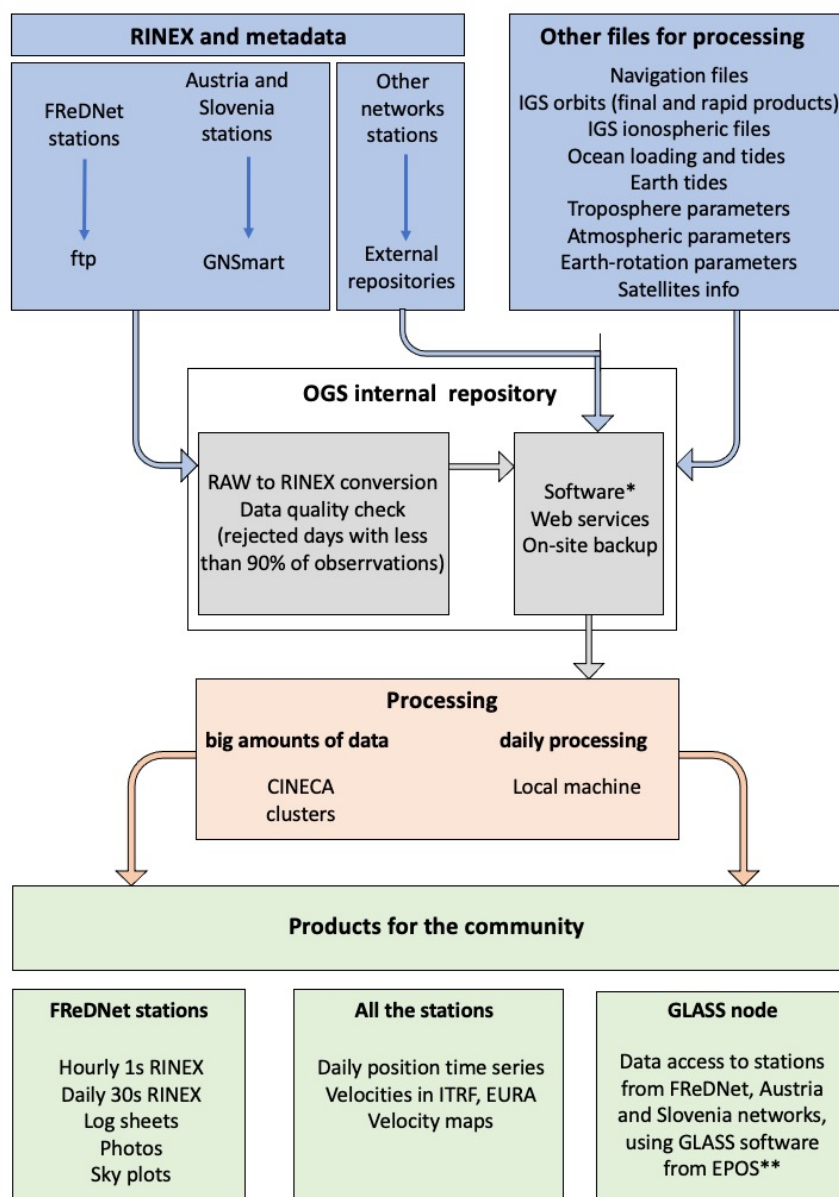
135

**Fig. 4: GNSS data flow at the OGS (Italy). *Software used: GAMIT/GLOBK ver10.71 (Herring et al., 2018) for GNSS data processing, GMT ver6.4.0 for plots and maps, GNSMART for downloading raw streams data from Austria and Slovenia networks and transform them into RINEX format data, TEQC (Estey and Meertens, 1999) for data quality check (it is end-of-life, but for GPS data it is still functional), Git ver2.27, free and open source system (https://git-scm.com/), for scripts updating and management**
140 **between different machines, Anubis ver2.3 (https://gnutsoftware.com/software/anubis) for sky plots and RINEX3 generation. ** https://glass.gnss-epos.eu/#/site**

Along with the data, log sheets containing station metadata (e.g. station location, monument type, terrain description, photos, etc.) are collected for each GNSS station. The primary information source for metadata are the log sheets in IGS format

145 (https://www.igs.org/formats-and-standards/) recovered through the public repository of each networks and from the "Metadata Management and distribution system for Multiple GNSS Networks" (M3G) (https://gnss-metadata.eu/site/index). If the network does not provide IGS log sheets, we extract the information from RINEX files header. Finally, we verify the compatibility among different sources of metadata, when available.

Piece of information retrieved from the metadata is the history of the equipment, which is useful for identifying

150 discontinuities/jumps on the time series. ~~For the *a priori* coordinates of the stations, we use this information to populate the list of offsets in the time series,~~ In particular, we defined the offsets in the time series for each station referring to (i) the information about the station equipment, which allowed defining an offset for each antenna change; (ii) the offsets reported by EUREF and IGS, and we excluded only offsets due to changes in processing procedure; (iii) the occurrence of earthquakes with magnitude greater than 5.0 reported by ANSS catalogue (U.S.G.S., 2017), thus we assigned offsets to each station inside

155 an empirical radius of influence depending on the magnitude (using the sh_makeeqdef program inside the GAMIT/GLOBK software, Herring et al., 2018).

Other important information reported in the log sheet of a GNSS site concerns the monument type and its location (on a building roof, on a building wall, or on the ground). The monument for a GPS/GNSS site should be designed to provide stable and secure support to mount the antenna. Therefore the monument should comply with a certain number of characteristics.

160 The IGS provides some recommendations for the monument itself and the monument site (https://files.igs.org/pub/station/general/IGS%20Site%20Guidelines%20July%202015.pdf). The material with which the monument is built should guarantee, within a reasonably low cost for building and maintenance, stability with time, corrosion resistance, long-term survivability, zero interaction with signal, resistance to frost action and temperature variations, with a minimum amount of metal in the proximity of the antenna. The site selected for placing the monument should be easily

165 accessible, clear of reflecting surfaces that can lead to multipath problems, with a shallow high-quality bedrock, clear horizon, with no local instabilities (the presence of faults, karstic cavities, the moisture content in soil rocks, or soil compression, should be checked), and with controlled vegetation. The monument site should finally be provided with continuous electric power and should guarantee data accessibility remotely (see also at https://kb.unavco.org/article/unavco-resources-permanent-gps-gnss-stations-634.html). It is not always easy to accomplish all these requirements, because of the difficulties in gathering all

170 the conditions and because the same environment changes with time, especially near urban areas due to urban developments. The consequences of not optimum site conditions likely reflect in the data quality, noisy time series, and increased uncertainties.
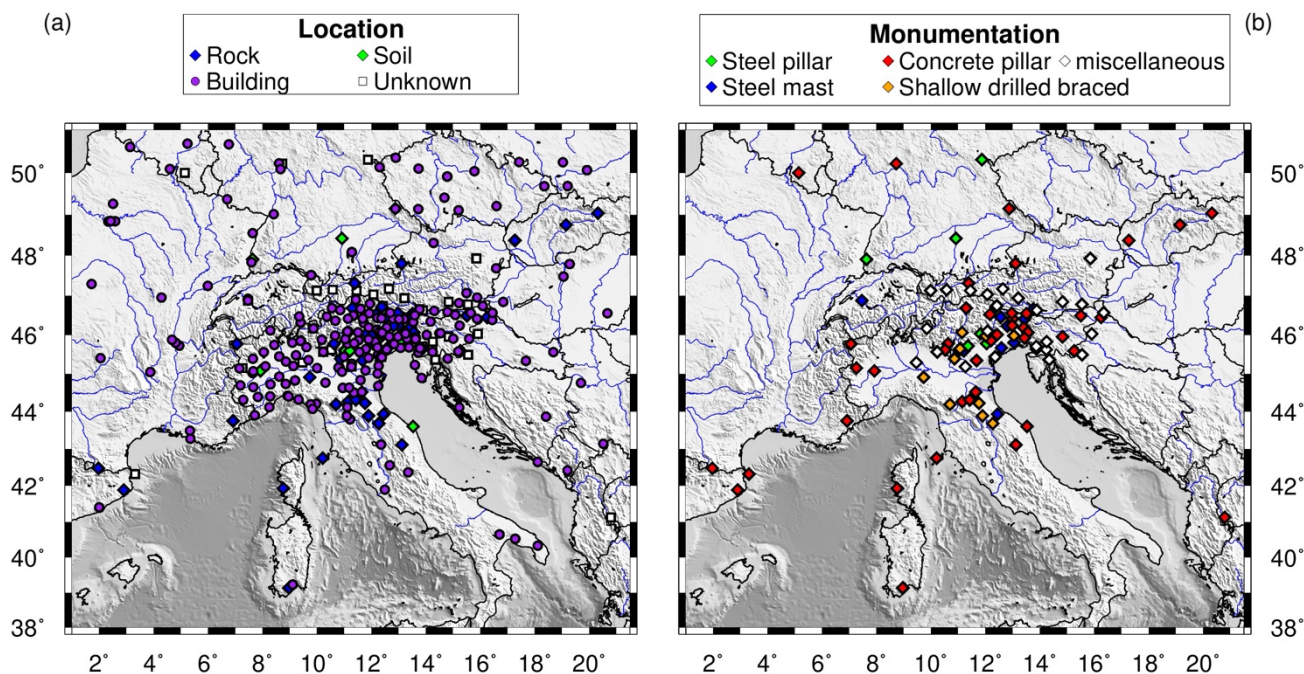
**Fig. 5: Information on the location and monument type of the GNSS stations considered in this study. a) Stations classified according to their location. Rock = site installed on hard terrain (not soil) or outcropping rocks. Building = site installed on a building or similar manufacts, like a wall, both on roof or fixed to the side wall. Soil = site installed on a soft terrain. Unknown = sites whose location description is incomplete or ambiguous. b) Stations not on buildings classified according to monument type. Steel pillar = monument made by a steel column. Steel mast = monument made by a steel bar. Concrete pillar = monument made by a concrete column with or without steel bars inside. Shallow drilled braced = monument consisting of a tripod drilled in the terrain). Miscellaneous includes mixed or not specified material.**

The log sheet of a GNSS site should ~~clearly report the monument's description~~ (material type, monument foundation, high and depth of the foundation, geological characteristics of the bedrock, spacing of eventual fractures in the bedrock, presence of faults nearby) ~~with a photo of it~~. However, log sheets are often incomplete and lack images. Figure 5 shows the monument information retrieved from the log sheets of our stations. Hence, we classify as anonymous the monument locations whose description in the log sheet is incomplete or ambiguous, and no photos or other sources of information are available to verify the data (Fig. 5a).

For stations installed on the roof or the wall of a building, we can assume that the stability is more affected by the edifice, than by the monument's composition (a steel mast or a concrete pillar). Therefore, we classify according to the monument material only the stations located away from buildings (Fig. 5b).

As can be noticed from the figure, the majority of stations are located on buildings/walls (251), and just one-third (107) of sites are located in the free-field (10 on soft soil, 57 on exposed rocks, and 40 are on unknown free-field locations). Approximately 50% of the latter have concrete pillars as monuments (54), ~10% have a monument composed of steel rods or

195     a steel tripod (shallow drilled braced, http://ring.gm.ingv.it/?page_id=43) (11), while of the rest, 9 have steel mast monuments, 6 have steel pillar equipped stations and 27 have not defined monument types.

## 3 Data processing

We process the GNSS data using the GAMIT/GLOBK software package (ver 10.71) (Herring et al., 2018). GAMIT can estimate station positions, atmospheric delays, satellite orbits, and Earth Orientation Parameters (EOP) from ionosphere-free

200    linear combination GNSS phase observables using double-differencing techniques to eliminate phase biases caused by drifts in the satellite and receiver clock oscillators. It outputs loosely constrained solutions (h-files) of parameter estimates and their covariance matrix. GLOBK is a module that implements Kalman filtering, and it is used to combine loosely constrained solutions (between networks and through time) and constrain the results into a consistent reference frame.

We process GPS data following these steps:

205   
- definition of sub-networks (subsets of stations);
- computation of loosely constrain solutions for each sub-network;
- combination of sub-networks solutions and computation of daily position for each station;
- computation of GNSS station velocities.

The RINEX files available each day are processed after being divided into subnetworks to ~~pursue~~ computational efficiency.

210    To do that, we use the netsel program of the GAMIT/GLOBK software package, which considers the geographic distribution of the stations in order to build the subnetworks (see Serpelloni et al., 2022 for a detailed description of the algorithm). Each subnetwork is linked to the next one by one station. An additional sub-network that contains two tie sites from each sub-network links all the sub-networks together. We perform some tests to identify the best nominal number of stations for each subnetwork, which depends on the total data available: we select 30 stations/subnetwork until 2008 and 40 stations/subnetwork

215    for the following years. ~~The data~~ from SLO_GPS are equipped with old receivers, ~~which~~ need to be elaborated using the LC_HELP algorithm of the GAMIT/GLOBK software, which uses an ionospheric constraint. To include these stations in the solution, we process them and some tie sites (TRIE, GSR1 and KDA2) in a separate sub-network. The tie sites of this sub-network will be excluded from netsel site list and then added to the tie sites sub-network.

~~We compute the loosely constrained solutions using GAMIT.~~ GPS phase data are weighted according to an elevation-angle-

220    dependent error model (Herring et al., 2018) using an iterative analysis procedure whereby the elevation dependence is determined by the observed scatter of phase residuals. The parameters of satellite ~~orbit~~ are fixed to the IGS final values. The first-order ionospheric delay is eliminated by using the ionosphere-free linear combination for all the stations except the SLO_GPS ones. Further details about models and parameters are reported in Table 1.

225

**Table 1: GAMIT solution parameters.**

| Parameter | |
|---|---|
| Processing mode | Baseline - orbits parameters are not estimated |
| Elevation cutoff | 10° |
| Magnetic field | IGRF13 (Alken et al., 2021) |
| Ionospheric model | 2nd-order ionospheric products - IGS IONEX files |
| Earth Orientation Parameters (pole position and UT1 and their rates of change) | Tightly constrained to *a priori* values obtained from IERS Bulletin A |
| Earth Rotation Model | IERS 2010 (Petit and Luzum 2010) |
| Solid Earth tides | IERS 2010 (Petit and Luzum 2010) |
| Ocean tidal loading | FES2004 (Lyard et al., 2006) |
| Atmospheric non tidal loading | Not applied |
| Atmospheric tidal loading | Not applied |
| *A priori* atmospheric parameters (pressure, temperature, zenith delay) | VFM1 grid (Vienna Mapping Function 1, Boehm et al., 2006) |
| Zenith delay estimation | estimates at 2-hr intervals for a 24hr session using a piecewise-linear (PWL) function |
| Tropospheric mapping function | VFM1 grid (Vienna Mapping Function 1, Boehm et al., 2006) |

230

The daily loosely constrained solutions of the subnetworks are combined and expressed in the International Terrestrial Reference frame (ITRF14/IGS14 by Altamimi et al. 2016; in particular, we use the newer GNSS geodetic reference frame IGb14) to obtain the position time-series of each station. We use a six-parameter Helmert transformation (translation and rotation) estimated by minimising the difference of positions of a set of stations with well-defined coordinates and velocities

235 as to *a priori* coordinates. We must keep both the coordinates and the EOP loosely constrained to do that. By visual inspection of the time series, we identify offsets that are unrelated to changes in the equipment or to earthquakes. We remove outliers automatically using two criteria similar to those of Floyd et al. (2010). First, we remove daily positions that have formal uncertainty greater than 20 mm. Then the time series were fitted to a model by a weighted linear regression to a model

consisting of a linear trend and offsets by using the ~~tsfit~~ program. Positions with residuals greater than three times the weighted

240 root-mean-square (RMS) value of the fit were also removed. Finally, from the analysis of the time series cleaned ~~from~~ the outliers, we estimated the random walk values for each site, and we identified ~~some sites to remove because of the noise level~~ ~~(random walk value greater than 2.0 mm²/yr)~~, applying the real_sigma algorithm (Floyd and Harring, 2019), which allows taking into account temporal correlations in the data.

We compute the velocities and coordinates of each station by combining all the cleaned daily solutions. In order to express the

245 solution in other reference frames (e.g., ETRF14, Altamimi et al. 2017), we need to estimate rotations and rotation rates independently of EOP since they are not included in the GAMIT solutions. Intending to reduce the computational time, we again divide the stations into sub-networks using netsel. We use a nominal number of 90 sites for each sub-network and the noise model obtained from the time series analysis. First, we estimated the velocities and positions of the included stations for each sub-network. Hence, we combine the solutions obtained for each sub-network in a unique solution expressed in IGb14.

250 Then, in a second step, we recompute the time series and velocities using, as *a priori* coordinates, the resulting values obtained in the previous iteration while extending the list of stabilisation sites to include all sites with random walk values lower than $0.5$ mm²/yr. Finally, we express our solutions relative to the Eurasia plate as defined by Altamimi et al. (2017) plate motion model (ETRF2014).

### 3.1 Computing infrastructure

255 Modern computational infrastructures allow the analysis of huge amounts of data with extraordinary advantages in terms of operational cost for data storage, processing and time-saving, leading to the timely provision of homogeneous products. We exploited the CINECA (https://www.hpc.cineca.it/) High-Performance Computing (HPC) resources to process and analyse in a very short time all the GNSS data available in the study area between 2002, January 1st and 2022, June 30th. We used the GALILEO100 Cluster, which is equipped with 554 compute nodes with 2 x CPU Intel CascadeLake 8260 each with 24 cores,

260 2.4 GHz, 384GB RAM DDR4. The job scheduling and workload management system is SLURM 21.08 (https://wiki.fysik.dtu.dk/niflheim/SLURM). SLURM is designed to accomplish three key functions: (i) allocation of exclusive/non-exclusive access to computing nodes to users for a specific duration of time; (ii) provision of a framework for managing the work (starting, execution, monitoring) on the set of allocated nodes; (iii) resources distribution handling by managing a queue of pending jobs.

265 Figure 6 aims to hint at the performance of CINECA clusters for GNSS data elaborations by reporting the calculation time on GALILEO100 compute nodes to obtain the GAMIT solutions ~~in the~~ function of the number of sites considered on each job sent to compute nodes. The figure shows that the calculation time varies on average with the square of the number of sites. Although the calculations of the GAMIT solutions are the most time-consuming jobs of the processing procedure, the total computation time on GALILEO100 depends not only on the number of available daily data but also on the adopted

270 parallelization strategy (i.e., the number of jobs sent to resources on compute nodes) and the occupancy of the machine (i.e. queue waiting time). In our study, we managed to process two decades of GNSS data in one week. We implemented the same

procedure described in the previous section on a local machine to process the data daily following the 30th of June 2022, with the aim of keeping the products updated. The daily processing is automated by using the crontab utility. More details on the implementation on the local machine can be found in the Appendix B.

275
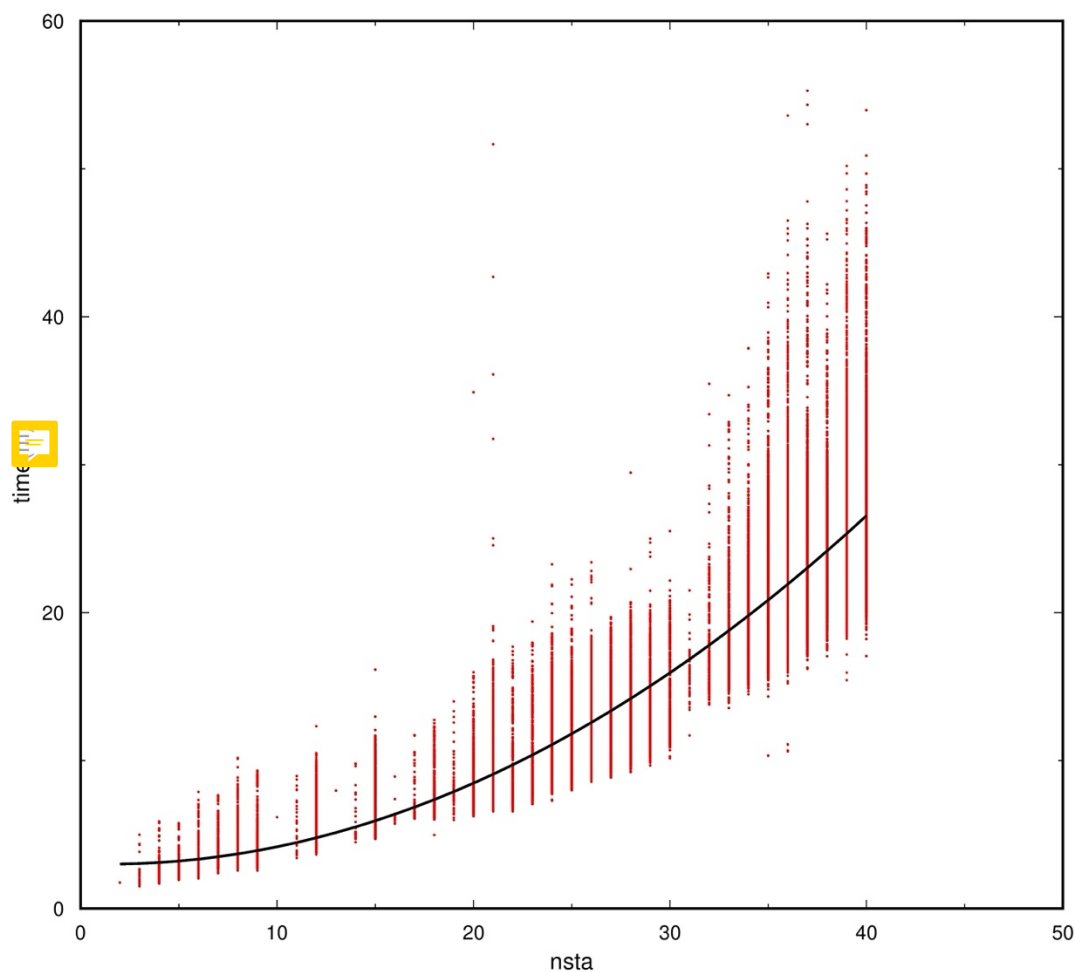
**Fig. 6: Calculation time for GAMIT solutions using GALILEO100 cluster in function of the number of sites (nsta).**

## 4 Geodetic time series and velocities dataset

This section ~~presents~~ the geodetic time series and velocity products provided. In support of the dataset, we illustrate several
280 tests performed to check the reliability of the documented results. For the sake of simplicity, we define the results of this study as "final time series" and "final velocities", and those estimations retrieved from the tests as "test time series" or "test velocities" .

## 4.1 Time series quality

We illustrate here the GNSS time series resulting from the data processing as a whole, whereas time series for single stations
285  are provided in the dataset, as explained above.
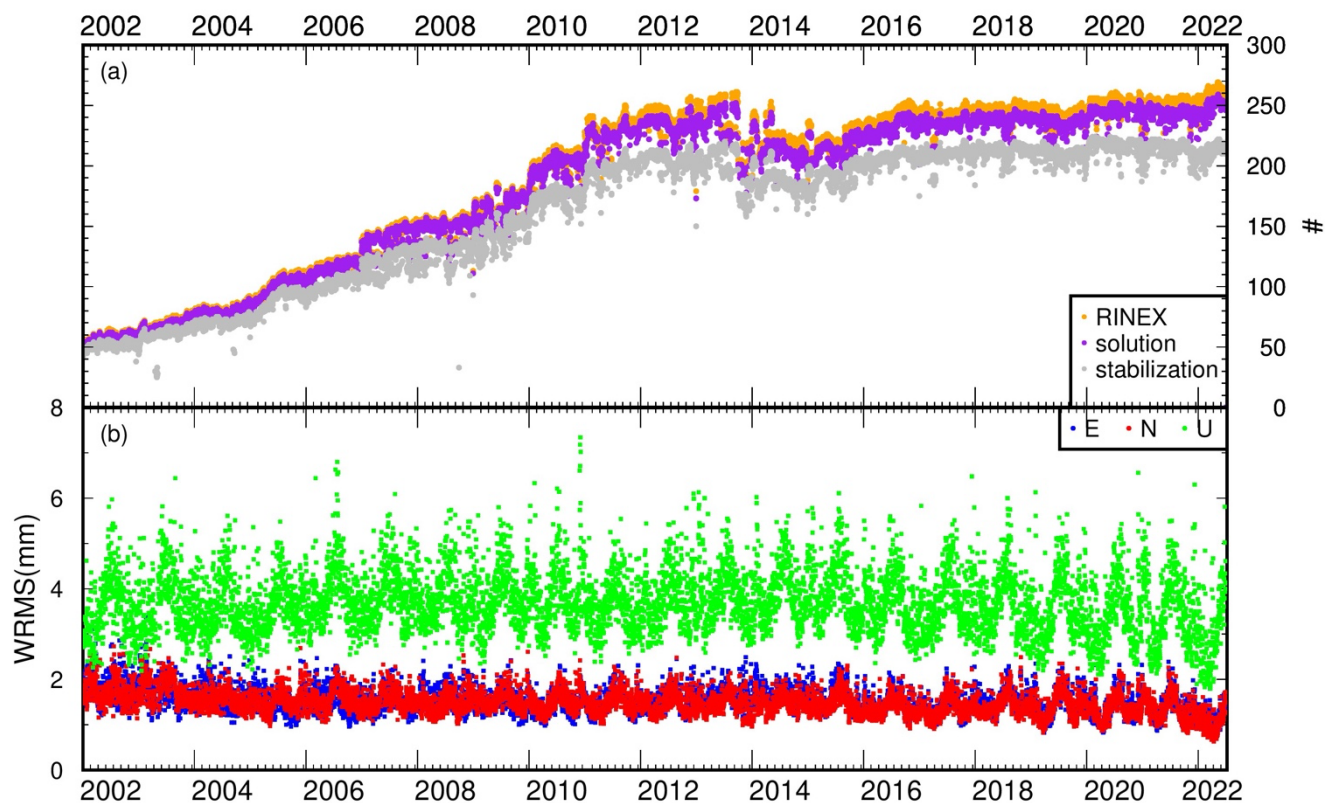
**Fig. 7: (a) Evolution of RINEX data available with time (orange dots), sites included in the solutions (purple dots) and sites being used in the reference frame realisation (grey dots); (b) weighted root-mean-square (WRMS) scatter of the fits to the coordinates of the reference frame stations in North (red), East (blue) and Up (green) components.**

290

The time-series length and quality depend on the number of good observations recorded at the sites, which is reflected in the
number of solutions obtained for each station. Figure 7 shows the evolution of RINEX available with time, the sites included
in the solution, and those being used in the reference frame realisation, along with the weighted-root-mean-square (WRMS)
of the fits to reference frame stations. Through data processing, the recorded RINEX allowed obtaining almost 97,1% of
295  solutions (purple dots in Fig 7a), a percentage which is indicative of the goodness of the dataset and of the adoption of an
appropriate processing strategy. The percentage of missing solutions (~ 3%) is mainly due to incomplete data records (RINEX
with less than 864 daily observations, i.e., with less than 30% of registrable daily observations) or stabilisation errors. As

illustrated in Section 3, in order to stabilise the solution we consider all sites with random walk value lower than 0.5 mm$^2$/yr, which led to consider as stabilisation sites ~ 80% of the available sites after 2011, and even ~ 90 % or more in the first decade

300    (grey dots in Fig. 7a). The average WRMS fit to the reference frame stations (Fig. 7b) is 1.7, 1.8, and 4.2 mm in North, East, and Up components, improving up to 20% in the latter since 2011, possibly thanks to the equipment improvements.

Figure 8 shows the stations' noise level through the representation of the WRMS of the time series and the RMS of the phase residuals. Notably, 90% of the stations show low noise levels, with values below 2 mm in the horizontal components and below 4.1 mm in the vertical one.
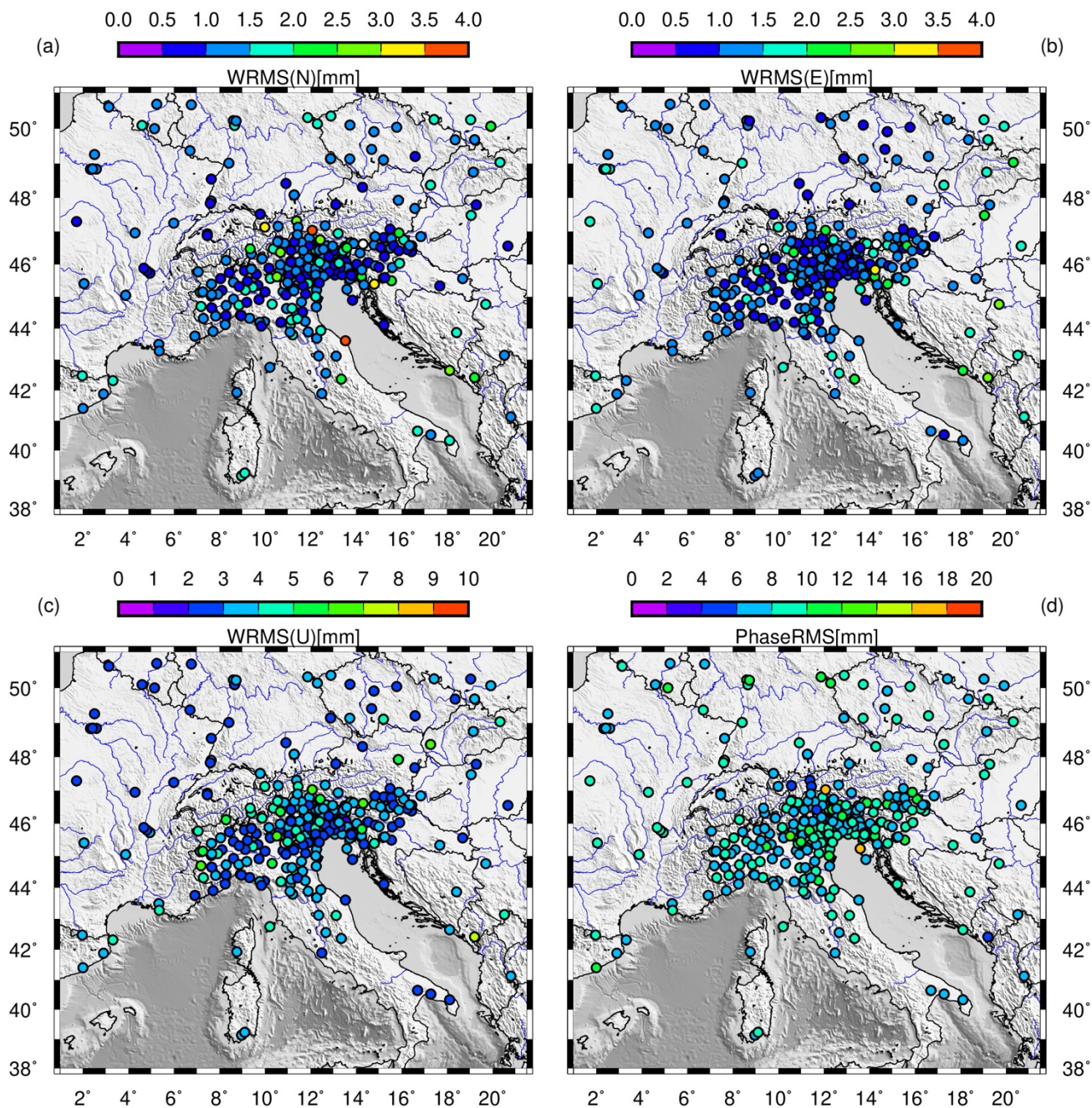
305

**Fig. 8: Time series WRMS in the horizontal (a, b) and vertical components (c ) and time series RMS of the phase residuals (d).**

## 4.2 Geodetic velocities

Time-series length is widely recognized as fundamental for defining the accuracy and precision of the estimated linear
310   velocities. For example, Blewitt and Lavallee (2002) show that 2.5 years of coordinate time series is the minimum span to
reduce velocity errors due to annual time series signals, primarily caused by surface loading due to hydrology and atmospheric
pressure However, the use of data spans greater than 4.5 years is preferable to eliminate velocity bias almost totally. Masson
et al. (2019) agree with this study, affirming that data spanning less than 4.5 years are not suitable for studies that require
precision lower than 1 mm/yr and that the best would be achieved by using long time-series (> 8 years length) which allow the
315   estimation of velocities with 0.2 mm/yr accuracy in the horizontal components and 0.5 mm/year on the vertical component.
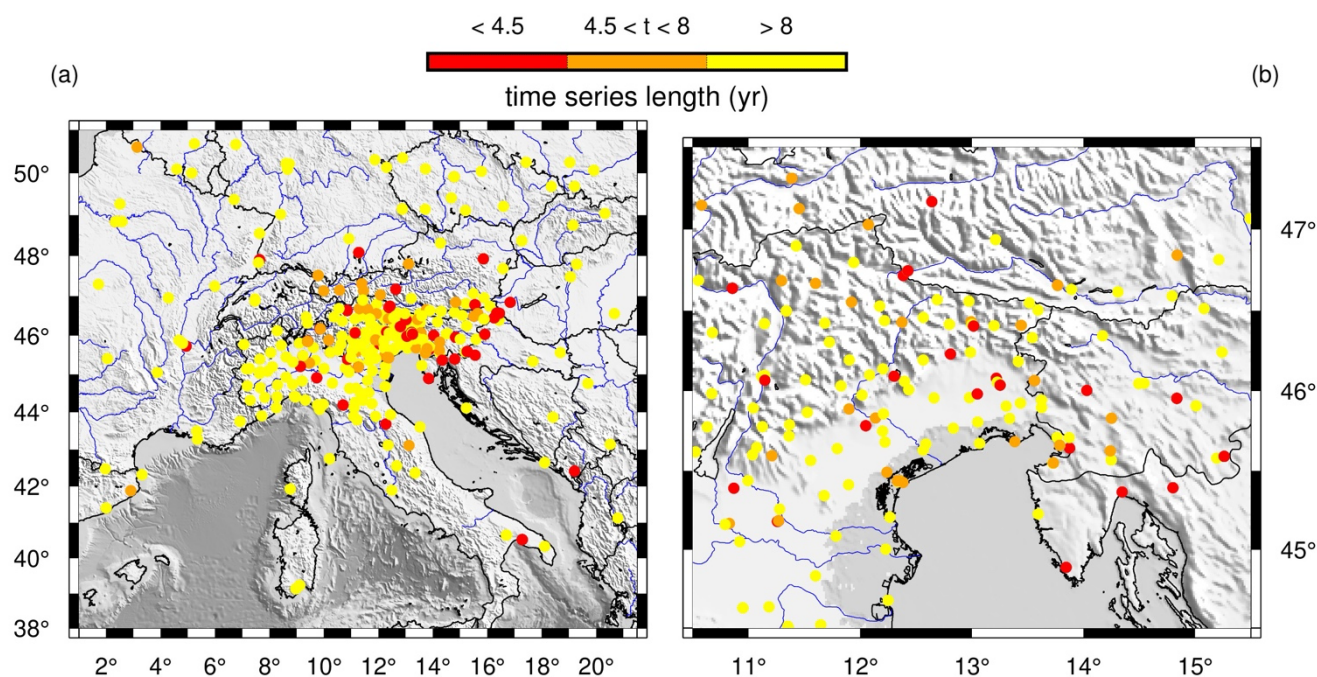
**Fig. 9: Time series length of the stations considered in this study.**

320   The stations considered in our study provide time series spanning from 0.27 (HELM) years to 20.49 years (between others, we
cite AQUI, GENO, GRAZ, GSR1, and TORI), as shown in Fig. 9. Most of the sites provide time series longer than 4.5 years
(84.4%), and even longer than 8 years length (69.4%), whereas just a small percentage are young stations providing coordinate
time series shorter than one year (8.9%). However, younger stations are often located in proximity to older stations, thus
allowing the retrieval of reliable and stable results also for that particular area (see Fig. 9b).

325

Data
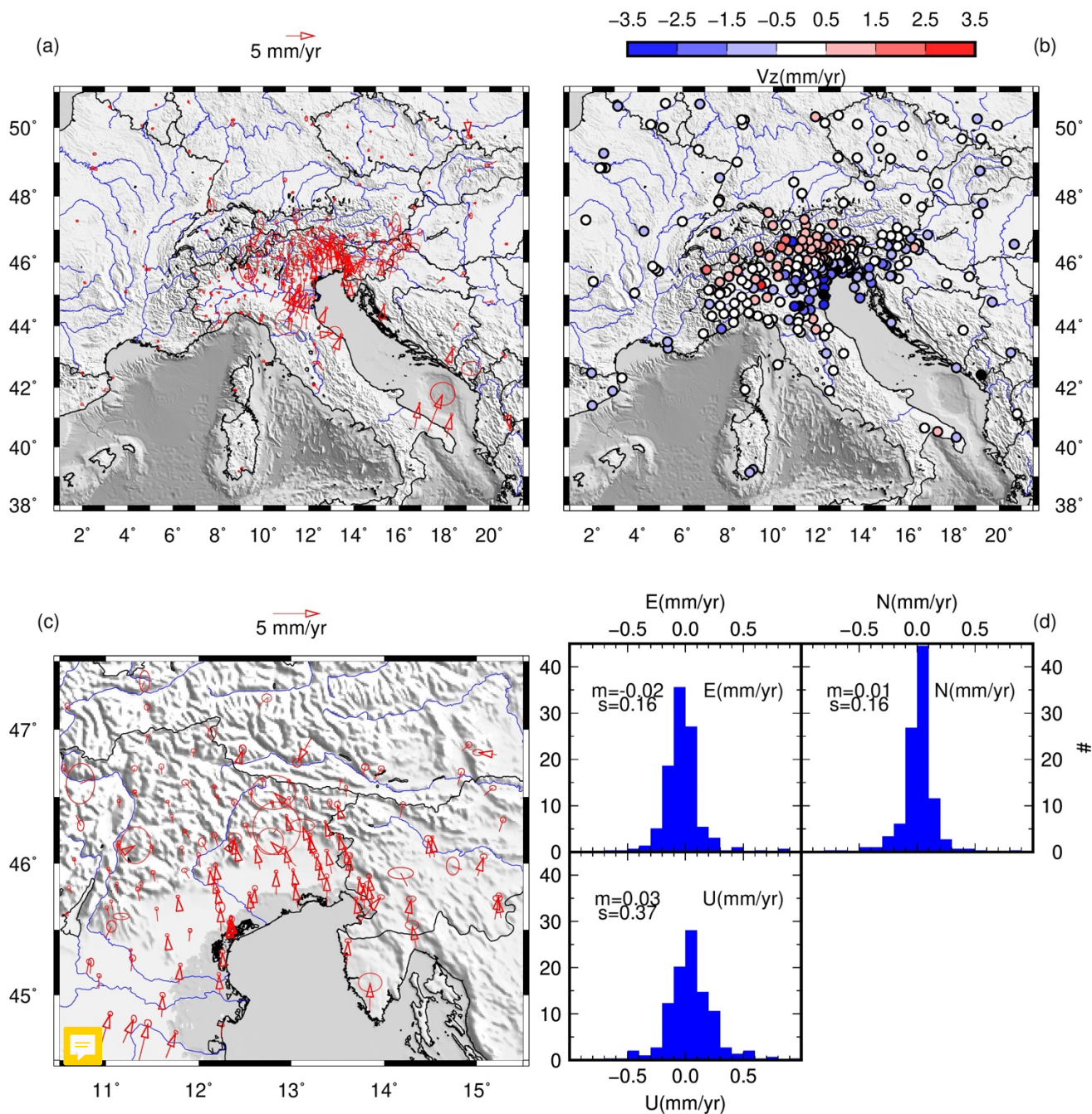
**Fig. 10: Estimated velocities with 95% confidence error ellipses, in the horizontal (a, c) and vertical components (b). (d) Histograms indicating the differences, along the three components, between velocity estimates calculated with GLOBK using the procedure described in Data Processing section, and those calculated using tsfit considering the stations with minimum 4.5 years long time series. Overall the differences are in a Gaussian shape, with mean and standard deviations values firmly below the mm/yr.**

We estimated the velocities and uncertainties of all stations for the horizontal (Fig. 10a) and vertical components (Fig. 10b) using GLOBK software. For completeness, we have also calculated velocities using tsfit, a program allowing a linear fit of the time series, and we have compared the results (Fig. 10d) finding sub-millimetre order differences. The estimated velocities in

335    ETRF14 show the active deformation in the Adriatic side of the Central Apennines, in the few stations located in the SE-Italy (Puglia region) and in the NE-Italy, with horizontal displacement directed to the North-East with values of 2-3 mm/yr in the Apennines and also in the Friulian plain and coast. NE-Italian Alps, instead, move with slower rates rounding 1 mm/yr. Significant horizontal motion is estimated in the SE-Italy, especially in the North velocity component, with 3.8 mm/yr and 4.2 mm/yr at USAL and MATE stations, respectively. The fastest motion (~ 7 mm/yr) is estimated at TARS and FATA stations

340    (located close to each other and indistinguishable at the scale of Fig. 10). However, this value is not reliable because these stations provide less than 1-year of observations, as it can be inferred from the high uncertainty. The estimated vertical displacement highlights the subsidence in the Po Basin (up to 3.5 mm/yr) and the uplift in the mountains, more accentuated in the Eastern Alps than in the Apennines. Beside the European reference stations located beyond Italian territory, also the stations in the NW-Italy show no significant displacement. The single exception is LODI station, whose anomalous behaviour (~ 2

345    mm/yr velocity in the horizontal components and ~ 2.8 mm/yr of uplift) is due to its location on the top of a depleted methane reservoir, recently converted into an underground gas storage facility (Priolo et al., under review). Zooming in the NE of the study area (Fig. 10c), a pattern of South-North decreasing velocities is distinguishable from the Friulian coastline and plain, to the Southern sector of the Eastern Alps, with an NNW orientation, whereas the stations located in Slovenia and Croatia show NNE oriented velocities. An anomalous south-directed motion is estimated in the OCHS station, in the Eastern Alps, likely

350    due to a landslide motion occurring along the slope where the GNSS station is located.

## 5 Evaluation of the quality and robustness of the dataset

Aiming to evaluate the quality and robustness of the dataset, we perform some experiments on the processing procedure, analyse the stations' quality, and compare our results with previous studies.

### 5.1 Data processing tests

355    Once time series, velocities and positions for each station were determined, we tested their stability and the reliability of the processing adopted procedure. For that, we performed a number of experiments on the available dataset to check for potential effects of selected options of the data processing with GAMIT/GLOBK (i.e., considering or avoiding tidal or non-tidal loadings or changing the stabilisation stations) on the results. In this way, if these tests do not highlight significant differences with the study results illustrated in the above sections, we can reasonably conclude that our results are reliable and not biased by

360    processing errors.

In one test, we changed the model used to estimate the atmospheric delay. Instead of using the default Vienna Mapping Function numerical weather model (VMF1) calculated by TU Vienna by interpolating hydrostatic and wet mapping function coefficients as a function of time and location (Boehm et al., 2006a), we adopt the Global Mapping Function (GMF) model developed by Boehm et al. (2006b) which fits the European Centre for Medium-Range Weather Forecasts (ECMWF) data

365    over 20 years. Then, since tides and non-tidal loadings are primary sources for time-variable displacements in station coordinates, we perform a test in which we consider the non-tidal atmospheric loading in the processing using a global gridded dataset provided by MIT and a further test, where we remove the ocean tidal loading that was inserted in the procedure described in Section 3. For all these three tests, we recalculated the time series for each station and compared them to the final ones, finding no significant dissimilarity, just slight differences ~~inferior to~~ 1 mm.

370    Regarding the velocity estimations, we recall here that one delicate step in the velocity estimation procedure is knowing how ~~to edit and weigh~~ the data, define, ~~and realise the reference frame. To do that~~, we need to consider what stations to include explicitly, how to treat the orbits and EOP, and practical constraints on computation speed and data storage. Although the GPS satellites provide a natural dynamic frame for ground-based geodesy, the doubly-differenced phase observations do not tie a ground station to the orbital constellation at the millimetre level ~~we require for scientific studies~~. ~~Instead, we~~ define and realise

375    a precise terrestrial ~~frame~~ by applying constraints to one or more sites in our network. To do that, we use the "generalised constraint" method of g[or], in which up to seven ~~Helmut~~ parameters (3 translations, 3 rotations, and 1 scale) are estimated such that adjustments to *a priori* values of the coordinates of a group of stations are minimised. For continental-scale networks like the one considered in this study, we estimate transla[tio]n and rotation and include as stabilisation sites a set of distributed stations for which we have good *a priori* values and sound data.

380    We perform some tests to check the goodness of the stabilisation frame considered. First, we conduct two tests on the first step of velocity estimation, using as stabilisation sites two different subsets of the reference sites set used in the final processing (see Test-1 and Test-2 in Fig. C1 in Appendix C). Secondly, on the second step of velocity estimation, we consider a regular grid of reference sites as stabilisation sites, generated considering a site every 2° (~ 222 km) (see Test-3 in Fig. C1 in Appendix C). Finally, we calculate the velocity field in our study area for each test. Overall, the mean difference values with respect to

385    final velocities are very low, which means up to 0.02 mm/yr in the North, up to 0.06 mm/yr in the East and Up to 0.14 mm/yr in the vertical component.

Finally, we perform two last experiments to evaluate the effects on the velocity results of introducing the periodic term (annual signal) in the coordinate time series fitting and applying a less restrictive criterion for outliers, i.e., 5 sigmas instead of 3 sigmas. The mean differences, with respect to the final velocities, are of the order of 0.02 - 0.03 mm/yr in both cases for

390    stations with at least 4.5 years of time series length.

## 5.2 Considerations on the stations quality

~~The time changes in the environment of the surroundings of~~ a GNSS station affect the RMS of the phase residuals. The ~~changes~~ can be related not only to climatic conditions, ~~with~~ an increase of weather perturbations due to climate change, but also to

urban developments in the proximity of the stations, manufact building, vegetation growth, radio-electronic sources
395    perturbations, traffic increase, etc. In Fig. 11 we plot the RMS variation with time for some stations. A seasonal increase of
the RMS is visible everywhere throughout the considered time interval.
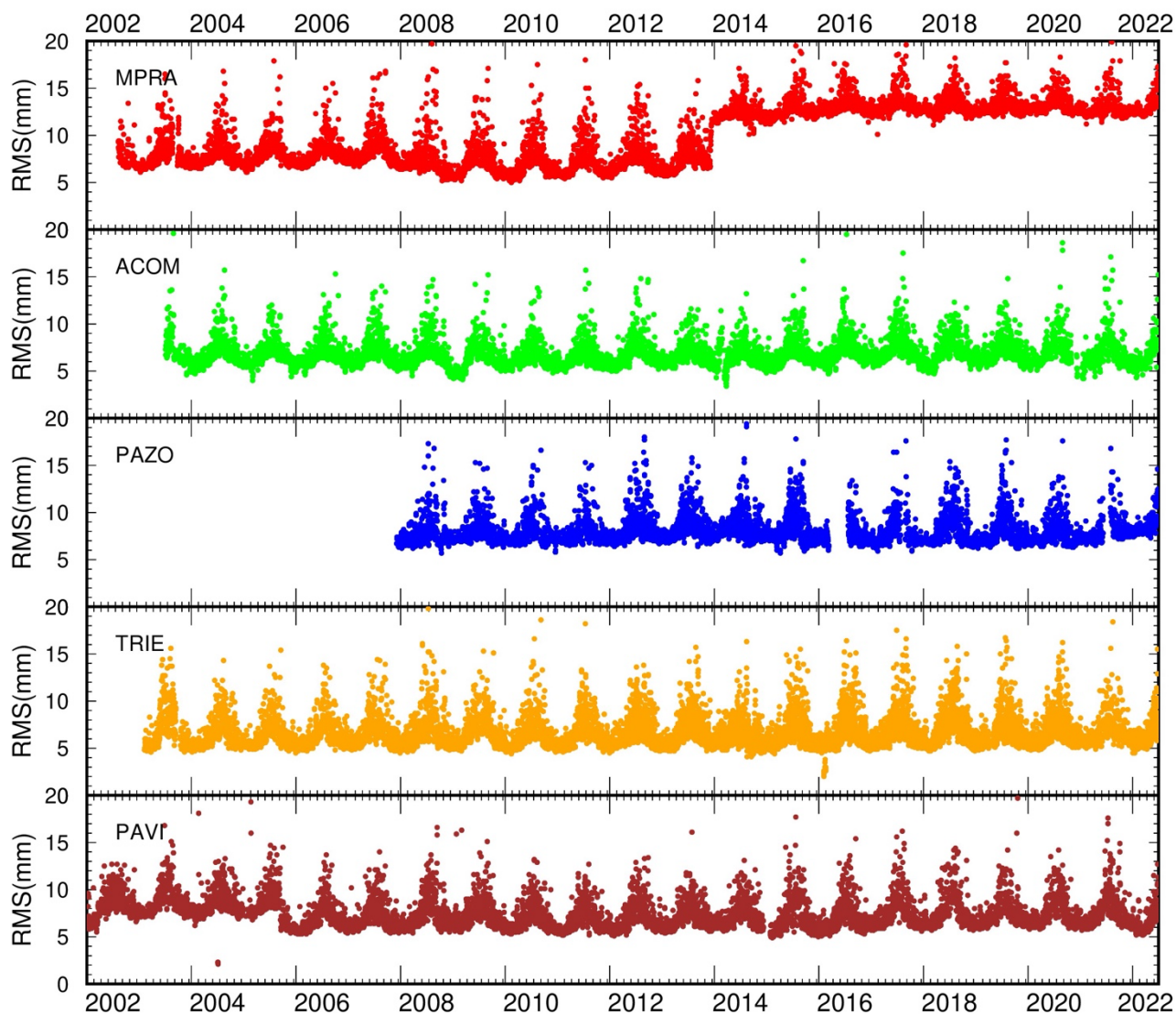
**Fig. 11: Variation of the RMS of the phase residuals with time of different GNSS stations.**

400

The phase RMS, typically 4-7 mm, increases up to 15-20 mm in July-August. This characteristic ~~regards whatever~~ station, ~~equally being~~ located near the coast (i.e., TRIE), or in the middle of the plain (as PAZO, PAVI) or in a mountain context (i.e., ACOM, located at 1774 m altitude; MPRA, located at 808 m altitude; ZOUF, located at 1946 m altitude). The same also occurs

405 at the stations in northern Europe; thus, it is a characteristic independent of geographic settings. A crosscheck on the sky plots shows that the phase RMS increases particularly during the daytime. We suspect it is due to ~~variable~~ atmospheric ~~noise~~. We certainly know that data from sites in the tropics have higher phase noise due to the higher water vapour content of the atmosphere. Orographic features such as mountain ranges are prone to produce a highly-turbulent and asymmetric atmosphere, which is challenging to model. In other words, tropospheric asymmetries associated with topography, such as being on a

410 mountain range's windward or leeward side, can produce asymmetrical time series scatter due to local-scale weather conditions (Materna and Harring, 2014).

Further considerations should be made for the MPRA station, which shows a systematic increase in the phase RMS since 2014. This condition is due to the construction of an electric tower in the proximity of the station, which has perturbed the site's noise level, leading to increased uncertainties, evident in the station time series (see Appendix A). Also PAVI station exhibits

415 a systematically different RMS of the phase residuals since the second half of 2005, showing a decrease of ∼ 2 mm. This decrease is likely due to a change in the equipment. The Trimble Zephyr Geodetic antenna (TRM41249.00), on day 14/09/2005 was substituted by a Leica choke ring antenna (LEIAT504) which features superior multipath rejection with uncompromised phase centre stability (<1mm) and is resistant to RF jamming ([http://uec-sigmat.com/Leica%20AT504%20(GG)%20Choke%20Ring%20Antenna%20-%20gps_gnss.html#productCollateralTabs1](http://uec-sigmat.com/Leica%20AT504%20(GG)%20Choke%20Ring%20Antenna%20-%20gps_gnss.html#productCollateralTabs1)).

420 However, the phase RMS decrease is not ~~so significant~~ as to be ~~reflected~~ in the uncertainty level, or evident in the position time series of the site (see PAVI time series in the dataset).

Many authors have investigated the contribution of geodetic monuments to GNSS time series noise properties (e.g., Herring et al., 2016; Langbein and Svarc, 2019 and reference therein). However, our dataset mainly comprises stations installed on buildings, and each class of free-field installation (as defined in Fig. 5) consists of a limited number of stations. Therefore,

425 obtaining reliable conclusions about the different free-field installation types is impossible. In Fig. 12, we compared the noise properties of the time series (WRMS of the three components and HRW) of stations installed on buildings with those of free-field installations. We conclude that the stations on buildings are not significantly different from the stations installed on outcropping rocks.
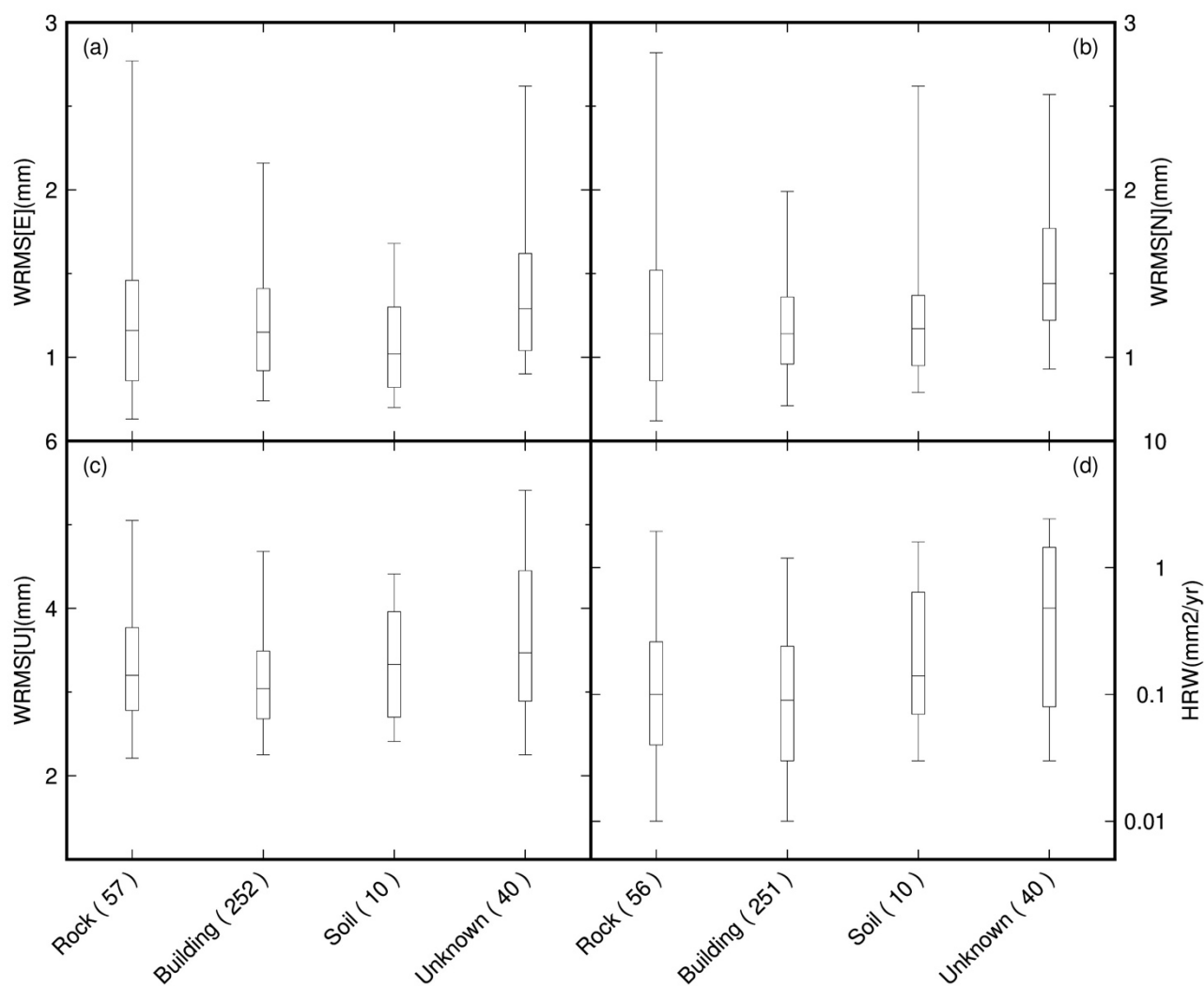
430 **Fig. 12: Box-and-whisker plots showing the distribution of the weighted-root-mean-square (WRMS) values estimated from the scatter of the station time series residuals along the East (a), North (b) and Up (c) components, and the equivalent horizontal random walk (HRW) represented the time-correlated noise. The line in the centre of the box is the median value, the boxes encompass 50% of stations (25th to 75th percentiles), the whiskers encompass 90% of stations (5th to 95th percentiles).**

## 5.3 Comparison with previous works

435

Different research groups published estimations of the velocity field in the area of interest of this study. Since the processing software or user-selected options can vary between different authors, through the comparison of our estimated velocities with those calculated by other researchers, we can evaluate the reliability of our solutions. If the misfits are not significant, we can

infer that our results are independent of data treatment and that our solutions are robust. On the contrary, if resulting velocities

440    are inconsistent between different studies, this can likely be ascribable to the differences in the data treatment performed. It would be complicated to discriminate which research group has provided the best estimate of the velocity field.

We compared our results with those calculated by the Nevada Geodetic Laboratory (NGL), downloaded in the IGS14 reference frame from http://geodesy.unr.edu/ on 2023, 3rd March, and by Serpelloni and co-workers, which recently published the surface velocity of the Euro-Mediterranean region (Serpelloni et al., 2022). NGL uses the MIDAS software (Blewitt et al.,

445    2016) to estimate the velocity field and automatically estimate the time series trend, identifying step discontinuities, outliers, seasonality and skewness in the data. Serpelloni and co-workers use the code of the Quasi Observation Combination Analysis (QOCA) software developed by JPL (https://qoca.jpl.nasa.gov) to analyse the time series and estimate the linear velocities. The comparison results are shown in Fig. 13 as histograms of solution differences. Overall, the mean differences are insignificant, ranging from 0.01 mm/yr to 0.04 mm/yr in the horizontal component and to 0.01 mm/yr and 0.17 mm/yr in the

450    vertical one, with standard deviation ranging from 0.18 mm/yr to 0.47 mm/yr. Slightly greater values are found compared to the NGL solution, especially in the Up component. These low discrepancies make us confident that our estimated velocities are robust and that the adopted data elaboration procedure is effective.
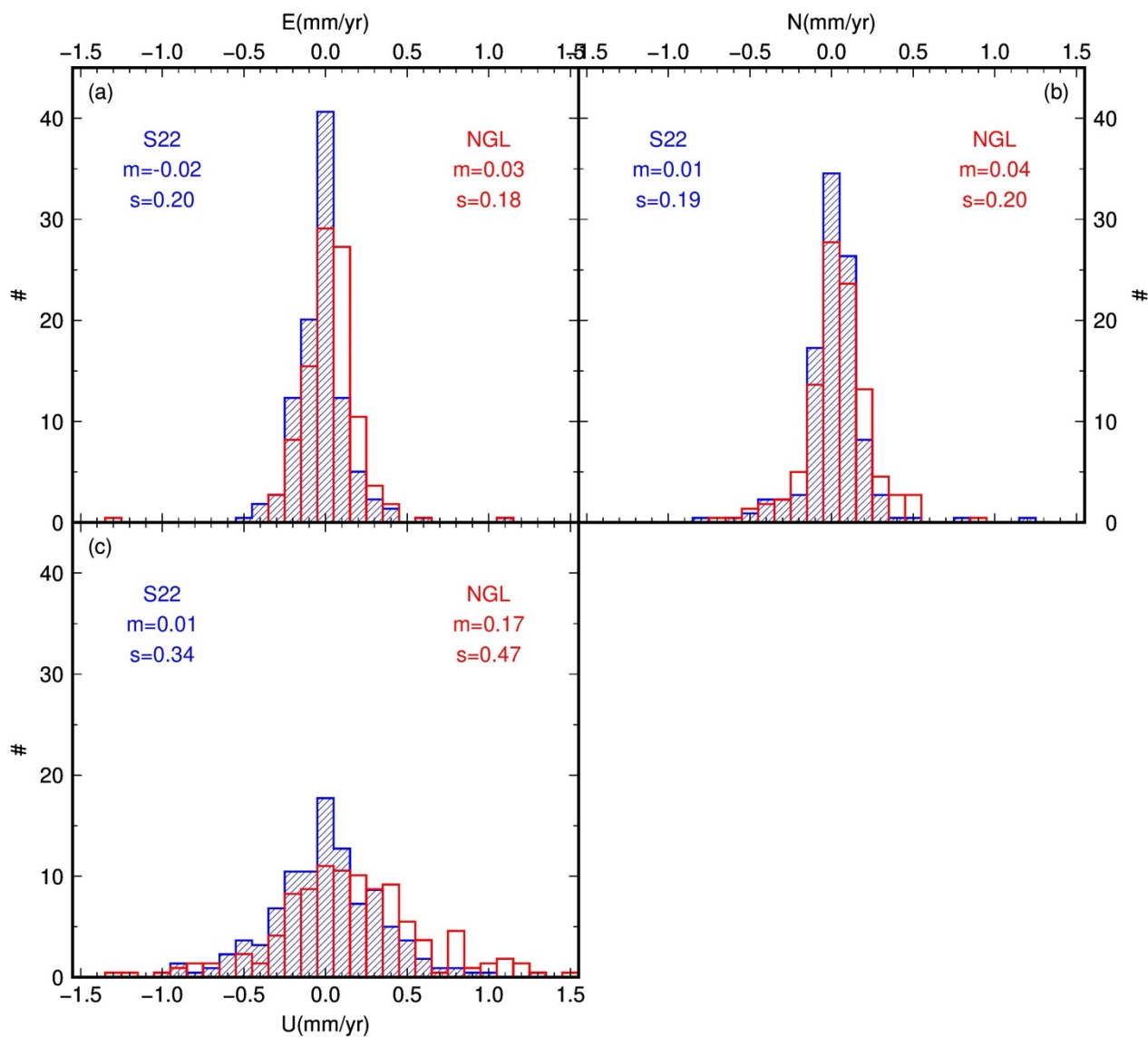
**Fig. 13: Histograms of the differences between the velocity values estimated in this study, along the three components, and those**
455 **estimated by Serpelloni and co-workers (S22, solution in blue colour) and by the Nevada Geodetic Lab (NGL, solution in red colour).**
**Only the stations with a minimum of 4.5 years have been taken into consideration for the histograms.**

**6 Data availability**

460 The geodetic time series and velocity dataset is accessible from the link https://frednet.crs.ogs.it/frednet_data/Projects/2022.OGS.GPS.solution/ or from the following DOI: https://doi.org/10.13120/b6aj-2s32 (Tunini et al., 2023). The products are distributed under a Creative Common licence CC BY-SA. The time series for each GNSS station, covering the 2002-2022 time interval (the last day processed is 2022, 30th June), are supplied in both international and Eurasia reference frames (ITRF14 and ETRF14). Besides the GNSS time series

465 plots, GAMIT/GLOBK pos-formatted files and ASCII formatted (Solution INdependent Exchange - SINEX) daily files are provided. Also, velocity values are provided in international and Eurasia reference frames (ITRF14 and ETRF14), and made available through tables and ASCII-formatted SINEX files. An annual update of the estimated velocities is planned, while daily updated time series will be available from the webpage https://frednet.crs.ogs.it/DOI/ by clicking on the "solutions" link. Further related information regarding the present paper (i.e. command files, information on jumps and discontinuities affecting

470 the time series due to earthquakes or equipment changes, station information, etc.) are provided at the same link of the dataset.

**7 Conclusions**

This paper ~~documents~~ ~~the results of~~ the processing of two decades of continuous GNSS ~~observation regarding~~ the slow convergent margin between the Eurasia and Adria microplate.

The dataset, available from the link https://frednet.crs.ogs.it/frednet_data/Projects/2022.OGS.GPS.solution/

475 (https://doi.org/10.13120/b6aj-2s32), contains the coordinate time series in both international and European reference frames, and velocity estimates for 350 permanent GNSS stations belonging to different regional and international networks, covering a time interval from 2002-01-01 to 2022-06-30. The time series are ~~provided cleaned out of unwanted values,~~ removed according to (i) formal uncertainties; (ii) residuals concerning the RMS of the fit value and (iii) noise level. The estimated velocity values result from combining all the cleaned daily solutions.

480 Other research groups have also estimated consistent geodetic velocity values, but the time series are rarely retrievable. Hence, the time series dataset presented here constitutes a crucial and complete source of information about the deformation of an active but slow converging margin over the last two decades. Furthermore, the resulting time series are currently calculated and stored daily in the framework of a long-term monitoring project, and are always available from the webpage https://frednet.crs.ogs.it/DOI/, whereas velocity solutions are planned to be updated annually. An overview of the employed

485 input data, GNSS stations information and data processing strategy, is documented.

The original input data are RINEX-formatted GNSS daily observations, sampled every 30s and processed using the GAMIT/GLOBK software package ver10.71. Data processing has been performed on the HPC cluster GALILEO100 from CINECA, which uses the SLURM system for job scheduling and workload management. Different experiments have been carried out on the same HPC cluster to evaluate the "goodness" of the processing procedure adopted and the solidity of the

490 solutions. The good results of the tests allow us to be confident that the dataset provided is accurate and robust, and it can be

used for high-precision deformation studies. In future studies, other GNSS systems data, such as Galileo or GLONASS observations, could also be included in the input data, providing more results and insights on the study region.

**APPENDIX A. The OGS geodetic network: FReDNet**

495 The Friuli Regional Deformation Network FReDNet (http://frednet.crs.inogs.it) is the OGS geodetic network established since the early 2000's in ~~the~~ NE-Italy ~~with the aim of monitoring~~ the distribution of crustal deformation and providing supplementary information for the regional earthquake hazard assessment (Zuliani et al., 2018). First stations of FReDNet were installed in 2002. Since then, FReDNet has grown until counting, nowadays, 22 permanent GNSS stations covering homogeneously the eastern Alps, the alluvial plain and the coastal areas of NE-Italy (Fig. 1). Most of the time series are longer than 15 years (Table
500 A1).

**Table A1. FReDNet stations specifics. MGBU station was installed on 2022, June 30th, therefore it is not included in the solution presented in the main text of the manuscript. UDIN is not operative anymore. H = hourly data sampled at 1s; D = daily data sampled at 30s; G = GLONASS satellites; R = RTK service; E = station belonging to EUREF Permanent Network (EPN) and data available**
505 **from official EPN website https://www.epncb.oma.be/_networkdata/siteinfo4onestation.php?station=ZOUF00ITA. Rock = site installed on hard terrain (not soil) or outcropping rocks. Building = site installed on a building or similar manufacts, like a wall, both on roof or fixed to the side wall. Soil = site installed on a soft terrain. *station name under definition; **dismissed in 2006.**

| | GNSS station | Antenna | Receiver | Operative since | Available services | Monument type | Location |
|---|---|---|---|---|---|---|---|
| 1 | ACOM | ASH701945E_M | TPS NET-G5 | 2003 | H, D, G, R | concrete pillar with steel rods | Rock |
| 2 | AFAL | ASH701945E_M | TPS GB-1000 | 2003 | H, D, G, R | concrete pillar with steel rods | Rock |
| 3 | CANV | ASH701945E_M | TPS NET-G5 | 2004 | H, D, G, R | concrete pillar with steel rods | Rock |
| 5 | CODR | ASH701945E_M | TPS NET-G3A | 2007 | H, D, G, R | steel mast | Building |
| 6 | FUSE | ASH701945E_M | TPS NET-G5 | 2007 | H, D, G, R | concrete pillar with steel rods | Rock |
| 7 | JOAN | ASH701945E_M | TPS NET-G5 | 2007 | H, D, G, R | concrete pillar with steel rods | Rock |
| 8 | LODI* | TPSCR.G5 | TPS NET-G5 | 2017 | H, D, G | miscellaneous | Soil |

| 9 | MDEA | ASH701945E_M | TPS NET-G5 | 2003 | H, D, G, R | concrete pillar with steel rods | Rock |
|---|------|--------------|------------|------|------------|--------------------------------|------|
| 10 | MGBU | TPSCR.G5 | TPS NET-G5 | 2022 | H, D, G, R | concrete pillar with steel rods | Rock |
| 11 | MPRA | ASH701945E_M | TPS NET-G5 | 2002 | H, D, G, R | concrete pillar with steel rods | Rock |
| 12 | NOVE | TPSCR3_GGD | TPS GB-1000 | 2009 | H, D, G, R | steel mast | Soil |
| 13 | PAZO | TPSCR.G3 | TPS NET-G3A | 2007 | H, D, G, R | steel mast | Soil |
| 14 | PMNT | TPSCR.G5 | TPS NET-G3A | 2015 | H, D, G, R | steel mast | Rock |
| 15 | SUSE | TPSCR.G3 | TPS NET-G3A | 2011 | H, D, G, R | concrete pillar with steel rods | Soil |
| 16 | TOLS | TPSCR.G5 | TPS GB-1000 | 2021 | H, D, G, R | steel mast | Building |
| 17 | TRIE | ASH701945E_M | TPS NET-G5 | 2003 | H, D, G, R | steel mast | Building |
| 18 | UDI1 | ASH701945E_M | TPS NET-G3A | 2006 | H, D, G, R | steel mast | Building |
| 19 | UDI2 | LEIAR20 | LEICA GR25 | 2010 | H, D, G, R | steel mast | Building |
| -- | UDIN** | ASH701975.01AGP | ASHTECH UZ-12 | 2002 | H, D | steel mast | Building |
| 20 | VALS | TPSCR.G5 | TPS NET-G5 | 2021 | H, D, G, R | steel mast | Rock |
| 21 | VARM | TPSCR.G5 | TPS NET-G5 | 2012 | H, D, G, R | steel mast | Rock |
| 22 | ZOUF | ASH701945C_M | TPS GB-1000 | 2002 | H, D, R, G, E | concrete pillar with steel rods | Rock |

510

As mentioned in the main text, data from FReDNet are collected, quality-checked, transformed into the RINEX-formatted data, and then released under a Creative Common licence (CC BY-SA), through a public ftp repository, as hourly and daily files at both 1s and 30s sampling. The repository is the FReDNet Data Centre (FReDNet DC 2016) accessible at the link https://frednet.crs.ogs.it/DOI/, where also metadata of FReDNet sites (log sheets in IGS format) are available. Pictures of

515 FReDNet stations are, instead, available on the FReDNet website http://frednet.crs.inogs.it. FReDNet provides real-time data as well, through the Real Time Kinematics (RTK) services, which allow reaching a centimetre-level accuracy in the positioning. The real-time data are available, free of charge, through the NTRIP (Networked Transport of RTCM via Internet Protocol) distribution server.

Most of FReDNet stations are installed on solid rock or firmly monumented in the thick pebbly layer of the alluvial plain,

520 whereas 5 of them (CODR, TRIE, UDIN, UDI1, UDI2) are located on the roofs of small buildings. All the stations are equipped with multi-frequencies and multi-constellations devices (Table A1). If the Topcon TPS GB-1000 and TPS NET-G3 receivers can track GPS and GLONASS satellite systems and just L1 and L2 frequency signals, the newest receivers TPS NET-G5 are capable of tracking GPS, GLONASS, Galileo, and Beidou satellites and the signals L1, L2 and L5.

During the installation phase of FReDNet sites, particular attention had been paid to the site monument, which is crucial for

525 providing a stable and secure support for the antenna and hence for ensuring the good quality of the data retrieved. The construction material should guarantee, within a reasonable low cost for building and maintenance, stability with time, corrosion resistance, long term survivability, ~~zero~~ interaction with signal, resistance to frost action and temperature variations, and ~~absence or minimum~~ amount of metal in the close proximity of the antenna. The site selected for placing the monument should be easy accessible, clear of reflecting surfaces that can lead to multipath issues, with clear horizon and controlled

530 vegetation, and based on a shallow high quality bedrock with no local crust instabilities (cracks, cavities, etc.). FReDNet sites were selected following the IGS recommendations, and periodically station maintenance is carried out to cut grown vegetation in proximity of the station or to restore the data connection. However, sometimes the environment changes with no possibility of restoring the initial conditions. One example is MPRA station. Though the initial location accomplished all the IGS requirements (https://files.igs.org/pub/station/general/IGS%20Site%20Guidelines%20July%202015.pdf), in 2014 an

535 electricity pylon was built in the proximity of the station, with consequences on the background noise level, as evidenced by increased error bars in the coordinate time series and in the phase RMS time series (Fig. A2). Nonetheless, our data processing strategy (illustrated in Section 3 of the main text) allows us to retrieve a stable solution, even with the presence of noise time series as the one provided by MPRA station.
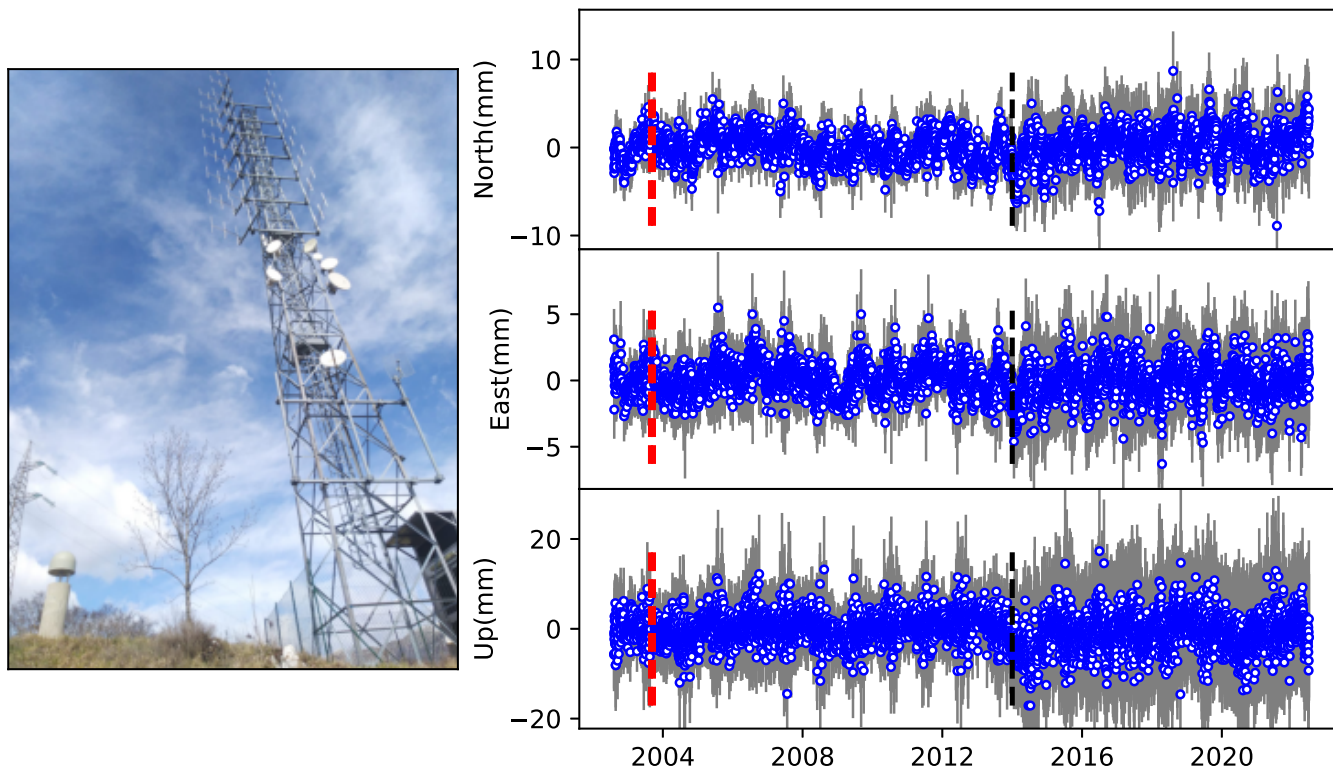
Fig. A1: MPRA station photo and time series of the residuals. Red dashed line indicates a change of the antenna, while black dashed line indicates the approximate date of the installation of the electricity pylon imaged in the photo.

## APPENDIX B. Daily local data processing

We implemented on a local machine the processing procedure described in the Section 3 of the main text with the aim to process the data following the 30th June of 2022. We have made the procedure automatic for daily processing. The local machine is a Mac mini equipped with Mac OS X (10.13) operative system. We use a crontab utility to manage the download of required input files, the update of metadata and the computation of daily solutions. From MIT, SOPAC, CDDIS and IGS repositories, we retrieve daily updates and files about orbits, atmospheric and tropospheric parameters, satellites aircrafts and ground station parameters, Earth orientation parameters, oceanic loading and tides, ionospheric and navigation files. RINEX files from FReDNet stations, EPOSA network and SLO_GPS stations are collected from OGS internal repositories. Observations from other networks are collected from the public data repositories of the networks, EPN data distribution services and EPOS service. The download of the observations is daily made also searching for eventual missing observations in the 21 days before the processing date, in order to remedy eventual data interruption or connectivity problems. Stations metadata are also downloaded periodically in the form of log sheets from the public data repositories of the networks or from the M3G service and used to update the station information file and the file with the discontinuity.

The automated procedure provides two types of time series for each GNSS station: i) coordinate time series obtained using IGS final orbit files (more precise) and ii) coordinate time series obtained using IGS rapid orbit files, which are less precise but available with just 3 days latency (https://cddis.nasa.gov/Data_and_Derived_Products/GNSS/orbit_products.html). In

560  particular, coordinate time series are calculated using final orbit files until 30 days before the processing date, and using rapid orbit files until 3 days before the processing date. An example of the resulting time series is given in Fig. B1.

Once the daily processing is finalized, an automatic e-mail message is sent to the data analysts with the summary of the processing results.

Finally, a periodic download of the latest tar-file containing incremental updates for GAMIT/GLOBK software is planned, in

565  order to keep the software updated. We plan also to update the velocity solution each year.
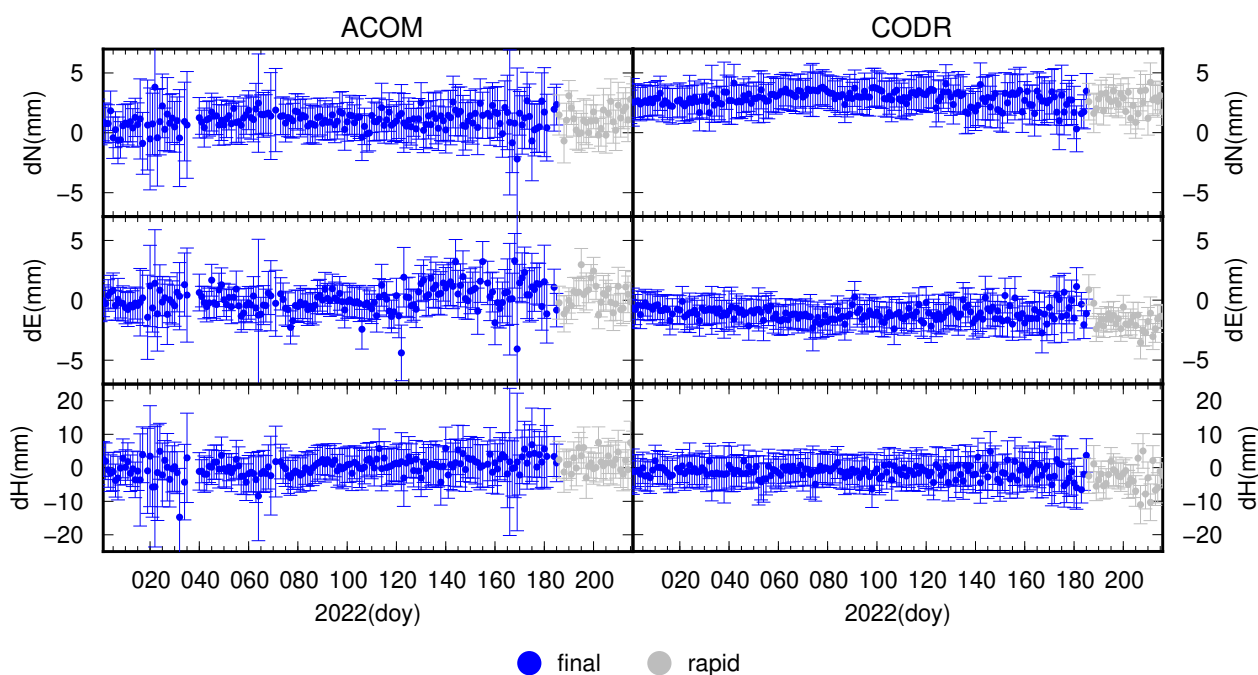
**Fig. B1: Coordinate time series in ETRF14 reference frame, calculated using final orbits (blue symbols) and rapid orbits (grey**
570  **symbols). Example for ACOM and CODR stations covering the time interval 2022-01-01/2022-08-04.**

## APPENDIX C. Reference sites
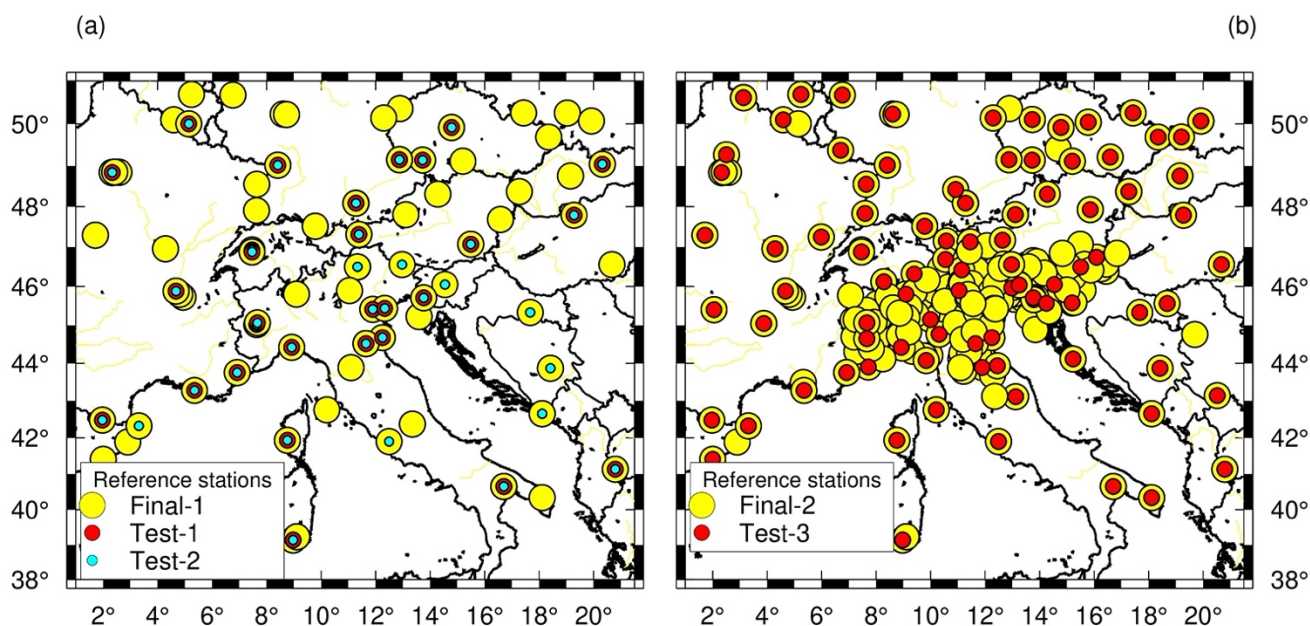
**Fig. C1: Reference sites used in the tests (Test-1, Test-2, Test-3) illustrated in Section 5.1, plotted as red and cyan circles, compared**
575 **to the reference sites used in the final processing (Final-1 and Final-2 indicate the first and second iteration, respectively, of the velocity calculation explained in Section 3), plotted as yellow circles.**

## Author contributions

DZ, GR, AM, LT developed the concept of this work. DZ developed the FReDNet network with the contribution of OGS
580 technical staff, and he set up the real-time data distribution service. AM, LT processed and elaborated the dataset, and prepared the manuscript and the figures. AM, LT, GR, DZ reviewed and edited the manuscript. All the authors have read and approved the submitted manuscript.

## Competing interests

The authors declare that they have no conflict of interest.

## Acknowledgements
585

This research was supported by OGS and CINECA under HPC-TRES program award number 2020-11. We acknowledge the CINECA award under the ISCRA initiative, for the availability of high performance computing resources and support (IscraC

IsC83_GPSIT and IsC96_GPSIT-2 projects). FReDNet is managed by OGS with support of the FVG Regional Civil Protection. We thank OGS staff for their support with the maintenance of the FReDNet GNSS network. We are grateful to all

590   public and private institutions that made the continuous GPS data used in this work available. We thank the GAMIT/GLOBK team at MIT for their continuous support. All figures have been made using the GMT software (Wessel et al., 2019), except for Fig. 4 made with PowerPoint (https://www.microsoft.com/it-it/microsoft-365/powerpoint) and for Fig. A1 made with Matplotlib (Hunter, 2007). Information on GMT can be found at: https://www.generic-mapping-tools.org/, information on GNSMART can be found at: https://www.geopp.de/gnsmart/, information on GAMIT/GLOBK can be found at:

595   http://geoweb.mit.edu/gg/.

**References**

Alken, P., Thébault, E., Beggan, C.D. Amit, H, Aubert, J., Baerenzung, J., Bondar, T.N., Browin, W.J., Califf, S., Chambodut, A., Chulliat, A., Cox, G.A., Finlay, C.C., Fournier, A., Gillet, N., Grayver, A., Hammer, M.D., Holschneider, M., Huder, L., Hulot, G., Jager, T., Kloss, C., Korte, M., Kuanh, W., Kuvshinov, A., Langlais, B., Léger, J.-M., Levur, V., Livermore, P.W.,

600   Lowes, F.J., Macmillan, S., Magnes, W., Mandea, M., Marsal., S., Matzka, J., Metman, M.C., Minami, T., Morschhauser, A., Mound, J.E., Nair, M., Nakano, S., Olsen, N., Pavón-Carrasco, F.J., Petrov, V.G., Ropp, G., Rother, M., Sabaka, T.J., Sanchez, S., Saturnino, D., Schnepf, N.R., Shen, X., Stolle, C., Tangborn, A., Tøffner-Clausen, L., Tob, H., Torta, J.M., Varner, J., Vervelidou, F., Vigneron, P., Wardinski, I., Wicht, J., Woods, A., Yang, Y., Zeren, Z., and Zhou, B.: : International Geomagnetic Reference Field: the thirteenth generation. Earth Planets Space 73, 49, doi: 10.1186/s40623-020-01288-x, 2021.

605

Altamimi, Z., Rebischung, P., Metivier, L., and Collilieux, X.: ITRF2014: A new release of the International Terrestrial Reference Frame modeling nonlinear station motions, J. Geophys. Res. Solid Earth, 121, doi:10.1002/2016JB013098, 2016.

Altamimi, Z., Métivier, L., Rebischung, P., Rouby, H., Collilieux, X.: ITRF2014 plate motion model, Geophysical Journal

610   International, 209(3),1906–1912, doi:10.1093/gji/ggx136, 2017.

Amante, C., and Eakins, B. W. (2009). ETOPO1 1 Arc-Minute Global Relief Model: Procedures, Data Sources and Analysis. NOAA Technical Memorandum NESDIS NGDC-24. Silver Spring: NOAA.

615   Battaglia, M., Zuliani, D., Pascutti, D., Michelini, A., Marson, I., Murray, M.H., Burgmann, R.: Network Assesses Earthquake Potential in Italy's Southern Alps, EOS, 84, 262–264, 2003.

Blewitt, G, and Lavallee, D. : Effect of annual signals on geodetic velocity, J. Geophys. Res., 107 (B7), 2002.

620 Blewitt, G., Kreemer, C., Hammond, W.C., and Gazeaux J.: MIDAS robust trend estimator for accurate GPS station velocities without step detection, Journal of Geophysical Research, 121, doi:10.1002/2015JB012552, 2016.

Boehm, J., Werl, B., and Schuh, H.: Troposphere mapping functions for GPS and very long baseline interferometry from European Centre for Medium-Range Weather Forecasts operational analysis data. doi:10.1029/2005JB003629, 2006a.
625

Boehm, J., Niell, A., Tregoning, P., and Schuh, H.: Global mapping function (GMF): a new empirical mapping function based on numerical weather model data Geophys. Res. Lett. 33, 2006b.

Bragato, P. L., Comelli, P., Sara., A., Zuliani, D., Moratto, L., Poggi, V., Rossi, G., Scaini, C., Sugan, M., Barnaba C., Bernardi,
630 P., Bertoni, M., Bressan, G., Compagno, A., Del Negro, E., Di Bartolomeo, P., Fabris, P., Garbin, M., Grossi, M. Magrin, A., Magrin, E., Pesaresi, D., Petrovic, B., Plasencia Linares, M.P., Romanelli, M., Snidarcig, A., Tunini, L., Urban, S., Venturini, E., Parolai, S.: The OGS - Northeastern Italy seismic and deformation network: Current status and outlook, Seismol. Res. Lett. 92, no. 3, 1704–1716, doi:10.1785/0220200372, 2021.

635 Braitenberg, C., and Zadro, M.: The Grotta Gigante horizontal pendulums - instrumentation and observations. Bollettino di Geofisica Teorica e Applicata, 40(3/4), 577–582, 1999.

Brancolini, G., Civile, D., Donda, F., Tosi, L., Zecchin, M., Volpi, V., Rossi, G., Sandron, D., Ferrante, G.M., andForlin, E.: New insights on the Adria plate geodynamics from the northern Adriatic perspective, Marine and Petroleum Geology, 109,
640 687-697, 2019.

Bressan, G., Barnaba, C., Peresan, A., & Rossi, G. Anatomy of seismicity clustering from parametric space-time analysis. Physics of the Earth and Planetary Interiors, 320, 106787, 2021.

645 Castellarin, A., & Cantelli, L.: Neo-Alpine evolution of the southern Eastern Alps. Journal of Geodynamics, 30(1-2), 251-274, 2000.

D'Agostino, N., Avallone, A., Cheloni, D., D'Anastasio, E., Mantenuto, S., and Selvaggi, G.: Active tectonics of the Adriatic region from GPS and earthquake slip vectors. J. Geophys. Res. 113:B12413. doi: 10.1029/2008JB005860, 2008.
650

D'Agostino, N., Cheloni, D., Mantenuto, S., Selvaggi, G., Michelini, A., and Zuliani, D.: Strain accumulation in the southern Alps (NE Italy) and deformation at the northeastern boundary of Adria observed by CGPS measurements. Geophys. Res. Lett. 32:L19306. doi:10.1029/2005GL024266, 2005.

655  Devoti, R., Esposito, A., Pietrantonio, G., Pisani, A. R., and Riguzzi, F.: Evidence of large scale deformation patterns from GPS data in the Italian subduction boundary. Earth and Planetary Science Letters, 311(3-4), 230-241, 2011.

Estey, L.H. and Meertens, C.M.: TEQC: The Multi-Purpose Toolkit for GPS/GLONASS Data and GPS Solutions; John Wiley & Sons: New York, NY, USA, Volume 3, pp. 42–49, 1999.

660

Floyd, M. A., and Herring, T. A.: Fast statistical approaches to geodetic time series analysis. In J. P. Montillet & M. Bos (Eds.), Geodetic Time Series Analysis in Earth Sciences Bos and Montillet, Springer Geophysics. Cham: Springer. doi:10.1007/978-3-030-21718-1, 2019.

665  Floyd, M. A., Billiris, H., Paradissis, D., Veis, G., Avallone, A., Briole, P., McClusky, S., Nocquet, J.M., Palamartchouk, K., Parsons, B., and England, P. C.: A new velocity field for Greece: Implications for the kinematics and dynamics of the Aegean, J. Geophys. Res., 115, B10403, doi:10.1029/2009JB007040, 2010.

FReDNet DC: Friuli Regional Deformation Network Data Center. Istituto Nazionale di Oceanografia e Geofisica
670  Sperimentale, Dataset, doi:10.6092/frednet, 2016.

Gerhard, W., Andreas, B., Martin, S.: RTK Networks based on Geo++ ® GNSMART—Concepts, Implementation, Results. In Proceedings of the International Technical Meeting (ION GPS−01), Salt Lake City, UT, USA, 11–14 September 2001.

675  Herring, T. A., Melbourne, T. I., Murray, M. H., Floyd, M. A., Szeliga, W. M., King, R. W., ... & Wang, L.: Plate Boundary Observatory and related networks: GPS data analysis methods and geodetic products, Reviews of Geophysics, 54(4), 759-808, 2016.

Herring, T.A., King, R.W., Floyd, M.A., and McClusky, S.C.: Introduction to GAMIT/GLOBK Introduction to
680  GAMIT/GLOBK, Release 10.7. Available at: http://geoweb.mit.edu/gg/docs/Intro_GG.pdf, 2018.

Hunter, J. D. : Matplotlib: A 2D Graphics Environment, Computing in Science & Engineering, vol. 9, no. 3, pp. 90-95, 2007.

Langbein, J., andSvarc, J. L.: Evaluation of temporally correlated noise in Global Navigation Satellite System time series:
685  Geodetic monument performance. Journal of Geophysical Research: Solid Earth, 124(1), 925-942, 2019.

Magrin, A., and Rossi, G.: Deriving a new crustal model of Northern Adria: The Northern Adria Crust (NAC) Model. Frontiers of Earth Science, 8, doi:10.3389/feart.2020.00089, 2020.

690  Masson, C., Mazzotti, S., Vernant, P.: Precision of continuous GPS velocities from statistical analysis of synthetic time series, Solid Earth, 10: 329–342, https://doi.org/10.5194/se-10-329-2019, 2019.

Matthews, K. J., Maloney, K. T., Zahirovic, S., Williams, S. E., Seton, M., and Müller, R. D.: Global plate boundary evolution and kinematics since the late Paleozoic: Global and Planetary Change, doi:10.1016/j.gloplacha.2016.10.002, 2016.

695

Petit, G. and Luzum, B.: IERS conventions, Tech. rep., Bureau International des Poids et mesures sevres (France), 2010.

Priolo, E., Zinno, I., Guidarelli, M., Romanelli, M., Lanari, R., Sandron, D., Garbin, M., Peruzza, L., Romano, A., Zuliani, D., Tunini, L., Magrin, A: The birth of an underground gas storage in a depleted gas reservoir - Results from integrated seismic

700  and ground deformation monitoring, JGR, under review.

Rossi, G., Pastorutti, A., Nagy, I., Braitenberg, C., and Parolai, S.: Recurrence of Fault Valve Behavior in a Continental Collision Area: Evidence From Tilt/Strain Measurements in Northern Adria, Frontiers in Earth Science, 9, 641416, 2021.

705  Serpelloni, E., Anzidei, M., Baldi, P., Casula, G., and Galvani, A.: Crustal velocity and strain-rate fields in Italy and surrounding regions: new results from the analysis of permanent and non-permanent GPS networks, Geophys. J. Int. 161, 861–880, doi: 10.1111/j.1365-246X.2005.02618.x, 2005.

Serpelloni, E., Cavaliere, A., Martelli, L., Pintori, F., Anderlini, L., Borghi, A., Randazzo, D., Bruni, S., Devoti, R., Perfetti,

710  P., and Cacciaguerra, S.: Surface Velocities and Strain-Rates in the Euro-Mediterranean Region From Massive GPS Data Processing, Front. Earth Sci., 10, 1–22, 2022.

Tunini, L., Magrin, A., Rossi, G., Zuliani, D.: GNSS time series and velocities about a slow convergent margin processed on HPC clusters: products and robustness evaluation [data set], https://doi.org/10.13120/b6aj-2s32 , 2023.

715

U.S.G.S., US Geological Survey, Earthquake Hazards Program: Advanced National Seismic System (ANSS) Comprehensive Catalog of Earthquake Events and Products: Various, https://doi.org/10.5066/F7MS3QZH, 2017.

Weber, J., Vrabec, M., Pavlovčič-Prešeren, P., Dixon, T., Jiang, Y., and Stopar, B.: GPS-derived motion of the Adriatic

720  microplate from Istria Peninsula and Po Plain sites, and geodynamic implications. Tectonophysics, 483(3-4), 214-222, 2010.

Wessel, P., Luis, J. F., Uieda, L., Scharroo, R., Wobbe, F., Smith, W. H. F., & Tian, D.: The Generic Mapping Tools version 6. Geochemistry, Geophysics, Geosystems, 20, 5556–5564. https://doi.org/10.1029/2019GC008515, 2019.

725     Zuliani, D., Fabris, P., Rossi, G.: FReDNet: Evolution of permanent GNSS receiver system. In: New Advanced GNSS and 3D Spatial Techniques Applications to Civil and Environmental Engineering, Geophysics, Architecture, Archeology and Cultural Heritage, Lecture Notes in Geoinformation and Cartography; Cefalo, R., Zielinski, J., Barbarella, M., Eds.; Springer: Cham, Switzerland, pp.123–137, 2018.